

Spatial and temporal variability of ice algal production in a 3D ice–ocean model of the Hudson Bay, Hudson Strait and Foxe Basin system

Virginie Sibert,¹ Bruno Zakardjian,² François Saucier,^{1,*} Michel Gosselin,¹ Michel Starr³ & Simon Senneville¹

1 Université du Québec à Rimouski, Institut des Sciences de la Mer, 310 Allée des Ursulines, CP 3300 Rimouski, Quebec G5L 3A1, Canada

2 Université du Sud Toulon-Var, Laboratoire de sondages Electromagnétiques de l'Environnement Terrestre, Bâtiment F, BP 20132, 83957 La Garde Cedex, France

3 Pêches et Océans Canada, Institut Maurice-Lamontagne, 850 Route de la Mer, CP 1000 Mont-Joli, Quebec G5H 3Z4, Canada

Keywords

Hudson Bay; ice algae; primary production; regional ocean model; sea ice.

Correspondence

Virginie Sibert, Université du Québec à Rimouski, Institut des Sciences de la Mer, 310 Allée des Ursulines, CP 3300 Rimouski, Quebec G5L 3A1, Canada. E-mail: virginie_sibert@uqar.qc.ca

doi:10.1111/j.1751-8369.2010.00184.x

* Deceased.

Abstract

Primary production, the basic component of the food web and a sink for dissolved inorganic carbon, is a major unknown in Arctic seas, particularly ice algal production, for which detailed and comprehensive studies are often limited in space and time. We present here a simple ice alga model and its coupling with a regional 3D ice–ocean model of the Hudson Bay system (HBS), including Hudson Strait and Foxe Basin, as a first attempt to estimate ice algal production and its potential contribution to the pelagic ecosystem on a regional scale. The ice algal growth rate is forced by sub-ice light and nutrient availability, whereas grazing and ice melt control biomass loss from the underside of the ice. The simulation shows the primary role of sea-ice dynamics on the distribution and production of ice algae with a high spatio-temporal variability in response to the great variability of ice conditions in different parts of the HBS. In addition to favourable light and nutrient conditions, there must be a sufficient time lag between the onset of sufficient light and ice melt to ensure significant ice algal production. This suggests that, in the context of enhanced warming in Arctic and sub-Arctic regions, earlier melt could be more damaging for ice algal production than later freezing. The model also includes a particulate organic matter (POM) variable, fed by ice melting losses to the water column, and shows a large redistribution of the POM produced by the ice ecosystem on a regional scale.

General circulation models (GCMs) all anticipate that global warming will be more rapid and intense in the Arctic and its ancillary seas compared with other regions of the globe (e.g., Holland & Bitz 2003; Gagnon & Gough 2005a,b). Recent observations support GCM predictions, showing large changes in sea-ice extent and thickness (Lindsay & Zhang 2005; Comiso et al. 2008), circulation and hydrography (Morison et al. 2000; Nechaev et al. 2004) and river discharges (Manabe et al. 2004) at high latitudes. The impacts of such environmental changes on key biogeochemical cycles, marine food web structure and ecosystem productivity are still not well-understood (IMBER 2005). Many polar species and marine food webs in general will be strongly affected because they are particularly well adapted to the specific environmental conditions that prevail in these areas (e.g., Smetacek &

Nicol 2005). In addition, marine ecosystems in polar regions are especially sensitive to any environmental change because of their low number of trophic links (Grebmeier et al. 2006; Moline et al. 2008).

Microalgae that colonize multi-year (Wheeler et al. 1996; Gosselin et al. 1997) and seasonal (Cota & Smith 1991a; Cota et al. 1991; Gradinger 2009) sea ice contribute significantly to polar ecosystem productivity. They can contribute as much as 25% of the annual total primary production (Legendre et al. 1992), corresponding to an estimated carbon production ranging between 5 and 15 g C m⁻² year⁻¹ on the Arctic basin scale (Arrigo 2003). Moreover, as phytoplankton and ice algal blooms do not coincide spatially or temporally (Lizotte 2003), the ice algal bloom extends the production period from 1 to 3 months annually (Michel et al. 1993). Therefore, sea-ice



algae probably represent an important food resource for higher pelagic (Runge et al. 1991) and benthic (Fortier et al. 2002) trophic levels, most notably when phytoplanktonic production is weak or lacking (Michel et al. 2002).

In the Arctic, most of the ice algal biomass accumulates in the bottom few centimetres of first-year sea ice (Smith et al. 1990). Ice algal growth is mainly controlled by the availability of light (e.g., Michel et al. 1988; Cota & Sullivan 1990; Gosselin et al. 1990) and nutrients (e.g., Cota et al. 1987; Gosselin et al. 1990). In response to extreme environmental conditions, ice algae have developed specific adaptations for growth and production. In particular, they possess a strong photoacclimation capacity as an adaptation to the very low light conditions induced by sea ice and snow cover (e.g., Cota 1985; Gosselin et al. 1985). These specific adaptations make them particularly sensitive to climate change, as even small changes in the duration and intensity of ice and snow cover will affect both their settlement and living conditions.

As a result of the harsh weather conditions and the remoteness that prevent extensive fieldwork, as well as the very heterogeneous physical regimes that may occur under ice cover, studies on ice algae are often limited in time and space. Understanding the links between climate forcing and ice algal dynamics at regional or basin scales would require comprehensive and detailed numerical modelling to fill the gaps in areas and times where key biogeochemical processes occur, but data are lacking (e.g., Arrigo 2003; Smetacek & Nicol 2005). However, models of ice algal dynamics are less advanced than planktonic models, and have generally focused on modelling ice algal growth in relation to sea ice thermodynamics (e.g., Lavoie et al. 2005; Nishi & Tabeta 2005, 2007; Jin et al. 2006; Jin et al. 2007). Most of these models have been developed in one dimension for a better comprehension of biological (growth) and environmental (inclusion, release) processes. This is the case in the work of Arrigo et al. (1993) and Arrigo & Sullivan (1994) on the Antarctic environment, as well as that of Lavoie et al. (2005) and Jin et al. (2006, 2007) for Arctic regions. The one-dimensional models of Jin and colleagues (Jin et al. 2006; Jin et al. 2007) and Lavoie et al. (2008) coupled sea ice and water ecosystems, adding new insight on the complexity of such coupling. Most of these models deal with the landfast ice environment, except that the model of Jin et al. (2007) is based on pack ice of the Bering Sea. The multidimensional model recently developed by Nishi & Tabeta (2005) for Saroma Ko Lagoon in northern Japan, and later adapted to the coastal region of the Okhotsk Sea, Japan (Nishi & Tabeta 2008), is the first to deal with spatial variability in a complex region.

We present here a simple ice alga model, and its coupling with a realistic sea ice–ocean regional model (Saucier et al. 2004) of the Hudson Bay system (HBS). This system, which includes Hudson Bay, James Bay, Hudson Strait and Foxe Basin, is one of the most important inland seas of the Arctic Ocean, receiving over 10^3 km^3 of freshwater per year from its drainage basin (Prinsenber 1986). The general circulation of the HBS is mainly cyclonic and forced by freshwater run-off, sea-ice melt during spring and summer (Prinsenber 1988), winds, semidiurnal tides and water fluxes from the Arctic Ocean and Labrador Sea (Ingram & Prinsenber 1998). The HBS is covered in ice for 8–9 months of the year. Changes in the timing of the freezing and melting of sea ice, which were anticipated by Martini (1986) and Ingram et al. (1996) as the most rapid consequences of climate warming in HBS, have recently been confirmed by observations showing that sea-ice melt actually occurs 2–3 weeks earlier now compared with the 1980s (Gagnon & Gough 2005a,b; Stirling & Parkinson 2006).

In the present paper, we will focus on the ecological robustness of the ice alga coupled model and the subregional variability of the simulated production cycle in response to the varied environmental conditions that prevail in the HBS. In addition, the modelling of release and sedimentation of the particulate organic matter (POM) produced by the ice ecosystem allows us to estimate its potential fate in the HBS, in response to circulation and mixing.

Material and methods

Hudson Bay sea ice–ocean model

A detailed description of the deterministic sea ice–ocean coupled model is presented in Saucier et al. (2004); here, we briefly summarize its major features. The Hudson Bay model domain (covering $1.24 \times 10^6 \text{ km}^2$) extends to the Labrador Sea in the east, north to Fury and Hecla Strait, and includes James Bay (Fig. 1). The spatial resolution is 10 km in the horizontal (polar stereographic projection) and 10 m on the vertical, with the surface and bottom-layer thicknesses adjusted to local sea level and topography, respectively. The ocean model is governed by the Navier–Stokes and hydrostatic equations, solved by a finite-difference scheme with 3D flux-corrected transport. It incorporates a 2.5-level turbulent kinetic energy model, supplemented with a diagnostic equation for the turbulent master length scale. This ocean circulation model is coupled to a multi-category dynamic elastic–visco–plastic (Hunke & Dukowicz 1997) and a two-ice-layer plus one-snow-layer thermodynamics (Semtner 1976) sea-ice model.

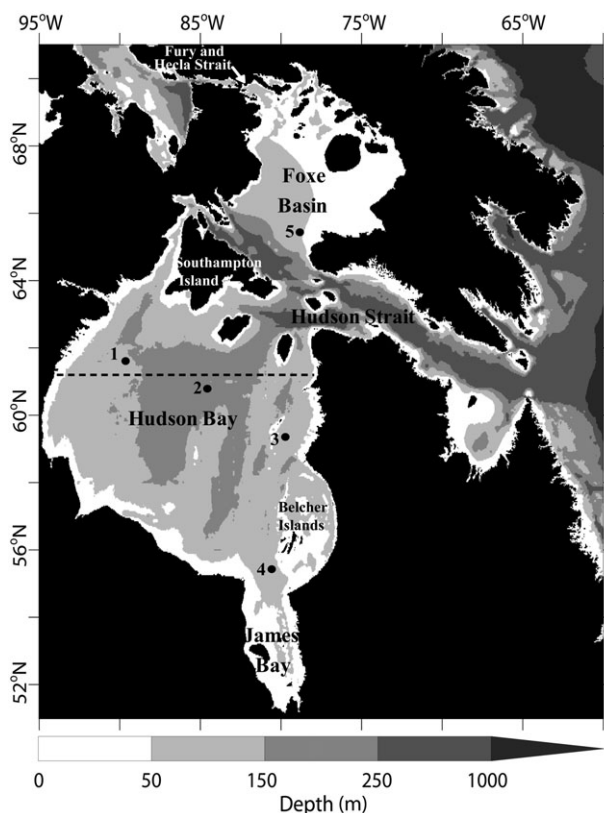


Fig. 1 Polar stereographic projection of the Hudson Bay marine system. Stations 1–5 have been used to extract high-frequency data for Fig. 10. The longitudinal dashed line indicates the transect we used to present the monthly variations of particulate organic matter concentration (see Fig. 11).

The sea-ice–ocean model is forced through 3-hourly atmospheric fields (surface air temperature, dew-point depression, surface winds, cloud cover and precipitation) provided by the Canadian Operational Weather Forecast Model. The heat and momentum fluxes between the ocean, the sea ice and the atmosphere are calculated by bulk aerodynamic exchange formulae. Run-off forcing is interpolated in time from daily run-off data in the 29 most important tributaries (HYDAT database, Environment Canada, http://www.wsc.ec.gc.ca/hydat/H2O/index_e.cfm). Boundary conditions east of Hudson Strait are prescribed by water levels with tidal constituents from Matsumoto et al. (2000), and monthly interpolated climatological temperature and salinity profiles from the Integrated Science Data Management group of Fisheries and Oceans Canada. Water levels at Fury and Hecla Strait are approximated from observations at Hall Beach Station (Canadian Hydrographic Service) for the tidal constituents, with a mean relative sea level of 20 cm tuned to obtain realistic inflow transport (see Saucier et al. 2004 for details). Temperature and salinity conditions are inter-

polated in time between simulated winter and summer mean values previously observed. The model computes fully prognostic solutions for turbulent kinetic energy, water level, currents, temperature and salinity fields, and sea-ice thickness and coverage. The simulations used here to drive the ice algal ecosystem are the same as in Saucier et al. (2004), and cover a 2-year period from August 1996 to July 1998. Comparisons of the model outputs to recent and historical observations have shown that the model produces a realistic seasonal cycle of the sea-ice–ocean environment in the HBS under the given hydrological and atmospheric forcing (e.g., Saucier et al. 2004).

Hudson Bay ice alga model

Our bottom ice ecosystem model considers the colonization of the lower 5 cm of the sea ice by algae and associated fauna. The two biotic compartments (i.e., the ice algae and ice fauna) are incorporated into the ice, whereas a dissolved inorganic nitrogen (DIN) compartment is included in the upper ocean layer. The dynamics of this process-based ecosystem model (using DIN for algal nutrient supply) is comparable with the dynamics of a nutrient–phytoplankton–zooplankton (NPZ) model. The ice algal growth model is similar to the one used in Lavoie et al. (2005) for the Canadian Archipelago, except that we include: (1) an ice faunal compartment; (2) an incorporation function to simulate the inoculation of algae and fauna during ice formation; and (3) ice algal photoacclimation processes. In contrast to Lavoie et al. (2005), the molecular diffusion across the ice–water interface is not considered in the present model because of the one-layer ice structure of the sea-ice model.

The parameters and functions used in the ice alga model are described in Tables 1 and 2. The rate of change in ice algal biomass is described by the following general equation:

$$\frac{dB}{dt} = (Inc \cdot B_0) + (\mu \cdot B) - (g \cdot Z) - (melt_loss \cdot B), \quad (1)$$

where *Inc* represents the incorporation rate of sea-surface algal biomass (B_0) into the sea ice, μ and B represent the ice algal growth rate and standing stock, respectively, g is the grazing function, with Z being the ice-faunal standing stock, and *melt_loss* is the sea-ice melt loss rate into the water column through ice melting. B_0 represents a background of algal biomass in the upper ocean water, and is considered to be a constant ($0.05 \text{ mmolN m}^{-3}$; Table 1). The incorporation rate (*Inc*) of sea-surface algae into the sea ice is set to zero for an ice thickness below 20 cm (i.e., for ice that is too thin to allow the formulation of a skeletal layer), and decreases exponentially as the ice grows (see Eqn. 1 in Table 2). This expression limits this

Table 1 List of parameters and variables of the model.

Name	Description	Value	Unit
δz	Bottom ice-layer thickness	0.05	m
Δz	Upper water column layer thickness	10	m
B	Ice algae	simulated	mmol N m ⁻³
Z	Ice fauna	simulated	mmol N m ⁻³
DIN	Dissolved inorganic nitrogen in the water column	simulated	mmol N m ⁻³
DIN_W	Sub-ice DIN concentration for the set-up simulations	1–10	mmol N m ⁻³
POM	Particulate organic matter	simulated	mmol N m ⁻³
Dep	Accumulated POM at the seafloor (see Fig. 13)	simulated	mmol N m ⁻²
PP	Ice algal primary production	simulated	mg C m ⁻² day ⁻¹
Lim_N	Nutrient limitation parameter (see Fig. 4)	simulated	Dimensionless
Lim_E	Light limitation parameter (see Fig. 4)	simulated	Dimensionless
PAR_0	Incident PAR	simulated	$\mu\text{mol photons m}^{-2} \text{s}^{-1}$
PAR_{subice}	Sub-ice PAR	simulated	$\mu\text{mol photons m}^{-2} \text{s}^{-1}$
H_{ice}	Sea-ice thickness	simulated	m
K_{ice}	Light attenuation coefficient of sea ice	1.5	m ⁻¹
H_{snow}	Snow thickness	simulated	m
K_{snow}	Light attenuation coefficient of snow	5	m ⁻¹
I_{conc}	Sea-ice coverage	simulated	dimensionless
$melt_loss$	Sea-ice melt loss rate	simulated	day ⁻¹
IML	Sea-ice melt velocity (see Fig. 2)	simulated	m day ⁻¹
Inc_{max}	Maximum colonization rate	0.24	day ⁻¹
B_0	Background algal concentration in the surface layer	0.05	mmol N m ⁻³
Z_0	Background fauna concentration in the surface layer	0.05	mmol N m ⁻³
μ	Ice algal growth rate	simulated	day ⁻¹
μ_{max}	Maximum growth rate	0.8	day ⁻¹
K_E	Half-saturation parameter	10	$\mu\text{mol photons m}^{-2} \text{s}^{-1}$
E_K	Photoacclimation parameter	simulated	$\mu\text{mol photons m}^{-2} \text{s}^{-1}$
$[Chla/C]_{\text{max}}$	Maximum Chla/C ratio	0.1	g Chla (gC) ⁻¹
α^{Chla}	P–E curve initial slope (photosynthetic efficiency)	0.06	g C (g Chla) ⁻¹ h ⁻¹ ($\mu\text{mol photons m}^{-2} \text{s}^{-1}$) ⁻¹
K_{DIN}	Half-saturation constant for DIN uptake	1	mmol N m ⁻³
g	Ingestion rate	simulated	day ⁻¹
g_{max}	Maximum ingestion rate	0.5	day ⁻¹
w	Ivlev constant for grazing function	0.05	(mmol N m ⁻³) ⁻¹
Asm	Ice-faunal growth efficiency	0.3	Dimensionless
$mort_z$	Maximum ice-fauna mortality rate	0.2	day ⁻¹
K_Z	Coefficient of vertical eddy diffusivity for DIN in the set-up simulations	1–10	m ⁻² day ⁻¹
Agg	Aggregation coefficient for sinking POM	10	m day ⁻¹ (mmol N m ⁻³) ⁻¹

entrapment process to the first stage of ice growth (i.e., late autumn–early winter), and assumes it is negligible during the ice algal bloom period. The ice algae growth term of the general equation (μ) depends on sub-ice irradiance (PAR_{subice}) and nutrient (DIN) availability in the ocean surface layer through a classic formulation for light and nutrient limitation, which assumes that they act in a multiplicative fashion (see Eqn. 2 in Table 2; e.g., Droop 1983).

The light available for ice algal photosynthesis (PAR_{subice}) is defined in Eqn. 3 of Table 2, using diffuse attenuation coefficients for ice and snow of 1.5 and 5 m⁻¹, respectively (Perovich 1996). We assume that most of the light attenuation occurs above the thin (ca. 0–5 cm) ice algal layer, and that chlorophyll *a* self-shading is negligible in the bottom ice layer. The above-ice incident

irradiance (PAR_0) is assumed to be 43% of the total short-wave incoming radiation, this having been calculated in the physical model as it is also used to drive sea-atmosphere and ice-atmosphere heat flux.

The photoacclimation of ice algae is formulated via an adaptative response through the chlorophyll *a* to carbon ratio (Chla/C) that varies in response to light, nutrient availability and temperature (e.g., Geider et al. 1997; MacIntyre et al. 2002). We used a modified version of the empirical relationship of Cloern (1995) that includes a nutrient limitation term, where the half-saturation constant for DIN (K_{DIN}) was set at 1 mmol m⁻³, as in the ice algae model of Arrigo & Sullivan (1994) (see Eqn. 4 in Table 2). In this equation, the half-saturation parameter (K_E) drives the curvature of the Chla/C versus the light curve, and was set at 10 $\mu\text{mol photons m}^{-2} \text{s}^{-1}$ (the same

Table 2 Biological and geochemical functions used in the coupled ice alga model.

Function	Description	Equation	Unit
<i>Inc</i>	(1) Incorporation rate of sea-surface algae or fauna into sea ice	$H_i \leq 20 \text{ cm}; Inc = 0$ $H_i > 20 \text{ cm}; Inc = Inc_{max} \exp(-20H_{ice})$	day^{-1}
μ	(2) Ice algal growth rate	$= \mu_{max} \cdot \left[1 - \exp\left(-\frac{PAR_{subice}}{E_k}\right) \right] \cdot \left(\frac{DIN}{DIN + K_{DIN}} \right)$	day^{-1}
PAR_{subice}	(3) Sub-ice PAR	$= PAR_0 \cdot \exp[-(K_{ice} \cdot H_{ice} + K_{now} \cdot H_{snow})]$	$\mu\text{mol photons m}^{-2} \text{ s}^{-1}$
$Chla/C$	(4) Chlorophyll <i>a</i> to carbon mass ratio	$= \left[\frac{Chla}{C} \right]_{max} \cdot \left[0.25 + 0.75 \cdot \exp\left(-\frac{1}{2} \frac{PAR_{subice}}{K_E}\right) \right] \cdot \left(\frac{DIN}{DIN + K_{DIN}} \right)$	g Chla (g C)^{-1}
E_k	(5) Photoacclimation parameter	$= \frac{C}{Chla} \cdot \frac{\mu_{max}}{\alpha^{Chla}}$	$\mu\text{mol photons m}^{-2} \text{ s}^{-1}$
F_B	(6) Release flux of ice algae into water column	$= melt_loss \cdot B \cdot \delta z$	$\text{mmol N m}^{-2} \text{ day}^{-1}$
g	(7) Ice-faunal ingestion rate	$= g_{max} \cdot w \cdot Asm \cdot \{1 - \exp[-w \cdot (B - 0.05)]\}$	day^{-1}
F_Z	(8) Release flux of ice fauna into water column	$= (melt_loss \cdot Z + mort_z \cdot Z^2) \cdot \delta z$	$\text{mmol N m}^{-2} \text{ day}^{-1}$
F_{DIN}	(9) Turbulent DIN flux in the upper water column	$= -K_z \cdot \frac{(DIN - DIN_w)}{\Delta z}$ in the set-up simulations, but driven by the physical model in coupled simulations	$\text{mmol N m}^{-4} \text{ day}^{-1}$
sed_{POM}	(10) POM sinking rate	$= Agg \cdot (POM)^2$	$\text{mmol N m}^{-2} \text{ day}^{-1}$
F_{Bcarb}	(11) F_B converted into carbon unit	$= F_B \cdot 79.5$	$\text{mg C m}^{-2} \text{ day}^{-1}$
GL	(12) Ice algal loss by grazing (see Figs. 3, 5)	$= -g \cdot Z \cdot 84 \cdot \delta z$	$\text{mg C m}^{-2} \text{ day}^{-1}$

value as in Lavoie et al. 2005 for low snow sites). This value ensures that there are no significant variations of either $Chla/C$ or the photoacclimation parameter (E_k) before late spring, which is further related to the maximum growth rate (μ_{max}) and the initial slope of the $P-E$ curve α^{Chla} (namely the photosynthetic efficiency, as defined in Platt et al. 1980), through Eqn. 5 in Table 2. This photoacclimation expression allows fourfold variations of the $Chla/C$ ratio, from 0.1 to 0.025 g/g, assuming a maximum $Chla/C$ ratio of 0.1 (Robinson et al. 1998). We assume a constant value of $0.06 \text{ gC(gChla)}^{-1} \text{ h}^{-1}$ ($\mu\text{mol photons m}^{-2} \text{ s}^{-1}$) $^{-1}$ for α^{Chla} (Table 1), corresponding to the median value measured for bottom ice algae in first-year Arctic landfast ice during the vernal season (Kirst & Wiencke 1995). Using an α^{Chla} value of 0.06 restricts the variation of the E_k parameter to a range of 10–25 $\mu\text{mol photons m}^{-2} \text{ s}^{-1}$.

Melting of the ice bottom induces a loss of ice algae into the water column. According to the thermodynamics of the sea-ice model (Saucier et al. 2004), melting can reach ca. 0–1.2 cm day^{-1} . This rate is scaled to the thickness (5 cm) of the colonized layer of the bottom ice (see Eqn. 6 in Table 2), leading to a loss term of ice algae of ca. 0–0.3 day^{-1} . It is assumed that as the ice algae are flushed into the water column, the remaining ice algal biomass is redistributed upward in a constant 5-cm layer.

In our model, the ice fauna controls the ice algal biomass accumulation (see Eqn. 1 above). The fauna living at the bottom of the sea ice are composed of micro-fauna (Michel et al. 2002), such as heterotrophic ciliates and heterotrophic dinoflagellates, and meiofauna (Nozais

et al. 2001; Wiktor & Szymelfenig 2002), such as nematodes and harpacticoides copepods, which are all gathered in the same ice fauna compartment. The rate of change of the ice fauna is expressed by the following equation:

$$\frac{dZ}{dt} = (Inc \cdot Z_0) + (Asm \cdot g \cdot Z) - (mort_z \cdot Z^2) - (melt_loss \cdot Z). \quad (2)$$

The ice fauna equation considers growth through incorporation (Inc) and grazing (g) on ice algae, and losses through melt process and mortality. Incorporation of ice fauna into sea ice uses the same equation as for ice algae (see Eqn. 1 in Table 2), and a background faunal concentration (Z_0) in surface water considered to be constant ($0.05 \text{ mmol N m}^{-3}$; Table 1). The growth is set with an assimilation efficiency (Asm) of 30% (Hansen et al. 1997) of the grazed biomass, with the remaining being considered as feeding losses that are rapidly regenerated (see the dissolved inorganic nutrient “DIN” equation below). Little is known of the grazing ability of this fauna, and therefore the ingestion rate (g) is formulated with a modified Ivlev-type function (see Eqn. 7 in Table 2) that is frequently used in nutrient–phytoplankton–zooplankton–detritus (NPZD) models (e.g., Franks et al. 1986). The mortality term is defined by a quadratic-type function to limit the occurrence of oscillations generated in such non-linear predator–prey systems (e.g., Edwards & Bees 2001). The melting rate is expressed in the same way as for ice algae (see Eqn. 8 in Table 2).

Using allometric equations, the maximum ingestion rates were estimated to range from 0.2 to 0.5 day^{-1} by

microfauna (Michel et al. 2002), and from 0.25 day^{-1} to 1.1 day^{-1} for meiofauna (Nozais et al. 2001). To our knowledge there are no other published ingestion rates by microfauna in the sea ice. In addition, sensitivity tests (not shown) showed that the timing of ice algal accumulation is not significantly impacted by a maximum ingestion rate within this value range. Subsequently, the maximum ingestion rate was fixed in the present study at 0.5 day^{-1} (Table 1).

The DIN equation represents the evolution of dissolved inorganic nitrogen concentration in the upper ocean layer ($\Delta z = 10 \text{ m}$ in the model). DIN concentration is driven by sea-ice–ocean nitrogen fluxes related to uptake by ice algae and regeneration of non-assimilated grazed biomass, as well as oceanic turbulent and advection fluxes from the underlying layers. For the set-up simulations, the equation is as follows:

$$\frac{dDIN}{dt} = \frac{\delta z}{\Delta z} [(1 - A_{sm}) \cdot gZ - \mu B] + \frac{F_{DIN}}{\Delta z}, \quad (3)$$

where the DIN fluxes between sea ice and the water column are scaled with the ratio $\delta z/\Delta z$, and the turbulent flux is defined with a simple diffusion equation (see Eqn. 9 in Table 2), using a background nutrient concentration for the underlying water column (DIN_w) and a constant coefficient of vertical eddy diffusivity (K_z). To get an overview of the sensitivity of the model to nutrient conditions that could occur in the HBS, we defined two extreme scenarios to be used in the set-up simulations: high nutrient availability (HN) and low nutrient availability (LN) scenarios. The HN scenario is considered to be a relatively turbulent system ($K_z = 10 \text{ m}^2 \text{ day}^{-1}$), such as can be observed in the north-western part of the bay (Saucier et al. 2004), with high nutrient availability ($DIN_w = 10 \text{ mmol m}^{-3}$). The LN scenario is considered to be highly stratified ($K_z = 1 \text{ m}^2 \text{ day}^{-1}$), with low nutrient concentrations ($DIN_w = 1 \text{ mmol m}^{-3}$), i.e., the situation close to the mouths of major rivers in southern Hudson Bay (Ingram et al. 1989; Hudon et al. 1996).

Set-up forcing and coupling with the 3D sea-ice–ocean model

The set-up of the sea-ice ecosystem model was first made using time series of spatially averaged physical forcing extracted from the 1996–98 simulation by Saucier et al. (2004) for the whole HBS. This forcing included 6-hourly ice thickness and coverage, ice-bottom melting and short-wave surface radiation. These data permitted us to test the robustness of the model and its sensitivity to biological parameters (grazing, photoacclimation, regeneration) and physical forcing

(snow thickness, turbulent nutrient fluxes) before it was coupled to the 3D ice–ocean model.

The coupling of the sea-ice ecosystem model with the 3D sea-ice–ocean model requires knowledge of sea ice-derived forcing (thickness, coverage), the transport of ice algal and faunal biomass within the moving sea ice and the scaling of sea ice–ocean biogeochemical fluxes. The sea-ice ecosystem is not implemented per se in the multi-category two-layer dynamic sea-ice model, but is rather defined on cell-averaged ice conditions (ice thickness and coverage). Ice algal and faunal transports are defined through a conservative advection scheme that uses the ice velocities driven by winds and ocean currents. We do not consider any redistribution of ice algal and faunal biomasses as a result of ice ridging, the impact of which is thus limited to its effect on light conditions through variability in ice thickness.

The DIN available for ice alga production is now an oceanic variable, i.e., subject to advection and mixing in the 3D oceanic model. Ice–ocean nutrient fluxes are defined as those in the set-up model, except that they are further scaled by the sea-ice concentration of each cell, i.e., the fraction, between 0 and 1, of ocean covered by ice. The DIN concentration is initialized using a DIN–salinity relationship resulting from previous observations presented by Anderson et al. (1969) in eastern Hudson Strait, and in unpublished data collected in the HBS during the “MERICA” 2003 cruise (M. Starr, Fisheries and Oceans Canada, unpubl. data).

The release fluxes of ice algae, and associated grazers, by ice melt and mortality from the sea ice (see Eqns. 6 and 8 in Table 2) supply the particulate organic matter (POM) compartment in the upper water layer. POM is an oceanic variable, subject to transport, diffusion and sinking in the 3D oceanic model. The simulation, which assumes no POM at the start of the simulation and no regeneration of this variable, hence describes the potential fate of organic matter produced by the ice ecosystem. The release fluxes are scaled to the fraction of the oceanic cell covered by sea ice, as for DIN flux. The accumulated POM in the upper water layer is then subjected to sinking towards the seafloor, with sinking rates defined with a quadratic function of POM concentration (see Eqn. 10 in Table 2) for each water layer distributed from the surface to the bottom of the ocean. The quadratic dependence on POM represents a non-linear increase of the effective sinking speed of POM with concentration resulting from the effect of aggregation of POM particles. Accumulating the sinking flux in the bottom layer of the water column at each gridpoint of the oceanic model allows us to estimate the quantity of POM reaching the seafloor on a yearly basis over the model domain.

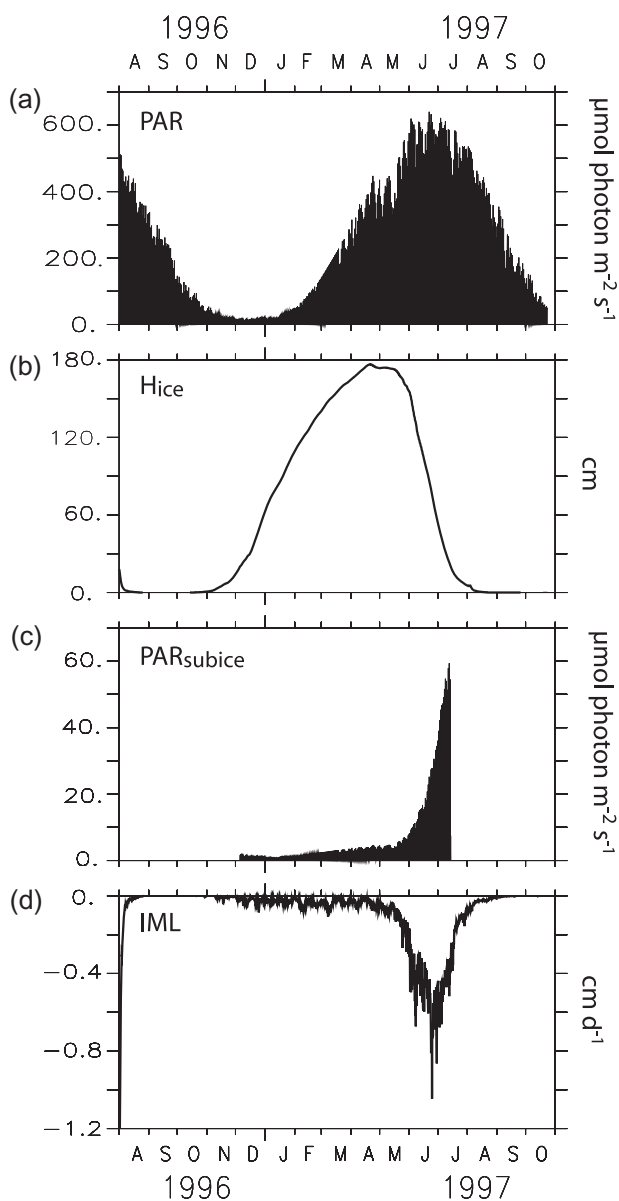


Fig. 2 Spatially averaged physical forcing for the whole Hudson Bay system (including Hudson Bay, James Bay, Foxe Basin and Hudson Strait) extracted from the sea ice–ocean simulation of Saucier et al. (2004). (a) Incident photosynthetically active radiations (PAR_0); (b) sea-ice thickness (H_{ice}); (c) sub-ice photosynthetically available radiation (PAR_{subice}); (d) bottom sea-ice melting velocity (IML).

Results

Mean seasonal cycles of ice algal production from the set-up simulations

Spatially averaged physical forcing extracted from the HBS ice–ocean model, and used to drive the set-up simulations, are shown in Fig. 2. The mean simulated daily

incident irradiance (upper panel) varies from high values (up to $600 \mu\text{mol photons m}^{-2} \text{s}^{-1}$) in late June to very low values (less than $10 \mu\text{mol photons m}^{-2} \text{s}^{-1}$) in December. The ice thickness starts to increase in early November, and reaches a maximum in April–May, with values close to 1.8 m. In our simulations significant ice melt starts in late May, reaching a maximum of 1.2 cm day^{-1} in late June during the rapid decline in ice thickness.

Incident irradiance and ice thickness primarily drive the irradiance available for growth of the bottom-ice algae. In these set-up simulations (Fig. 2), we assume the absence of snow and we set sub-ice irradiances to zero for ice thicknesses of less than 0.2 m. This is to reflect the hypothesis of unfavourable conditions for the algal colonization of the bottom sea-ice layer when the ice is too thin. As a result of decreasing incident irradiance and growing ice thickness, the sub-ice irradiance dramatically decreases in late autumn–early winter to a minimum of $1\text{--}2 \mu\text{mol photons m}^{-2} \text{s}^{-1}$ in mid-January. Afterward, it increases slightly because of increasing incident irradiance, but remains low ($<5 \mu\text{mol photons m}^{-2} \text{s}^{-1}$) because of continuously increasing ice thickness until the end of April. It is only in late spring–early summer that ice thinning because of melt leads to a major increase in the sub-ice irradiance, increasing from $3\text{--}4$ to $35 \mu\text{mol photons m}^{-2} \text{s}^{-1}$ between the end of May and late July.

This seasonal cycle of mean physical forcing (ice thickness, incident and sub-ice irradiance) compares well with those reported in other Arctic and sub-Arctic areas (e.g., Suzuki et al. 1997; Lavoie et al. 2005; Werner et al. 2007). Melting rates ($<1.2 \text{ cm day}^{-1}$) are also in good agreement with previous observations, i.e., 1.5 cm day^{-1} in Lavoie et al. (2005), and up to 10 cm day^{-1} in Hall & Rothrock (1987) and Sirevaag (2009). It is important to remember that these values are averaged for the whole HBS (including James Bay, Foxe Basin and Hudson Strait), and do not reflect the strong spatial variability of ice conditions found over the whole system.

Figure 3 shows the general behaviour of the sea-ice ecosystem model under the two distinct nutrient scenarios (see the earlier section on the Hudson Bay ice alga model). Under the HN scenario, the simulated ice algal production never becomes nutrient limited ($DIN > K_{DIN}$). Ice algal production (PP) only depends on light availability, and begins increasing in March, when PAR_{subice} reaches half of the photoacclimation parameter (E_k) (Fig. 4; $E_k = 6$, $PAR_{subice} = 3\text{--}4 \mu\text{mol photons m}^{-2} \text{s}^{-1}$). The ice algal production period continues until June, with maximal simulated biomass ($55 \text{ mg Chl}a \text{ m}^{-2}$) and primary production ($100\text{--}125 \text{ mg C m}^{-2} \text{ day}^{-1}$) occurring from mid-April to mid-May. Under this HN scenario, the ice algal biomass is successively controlled by grazing and melt losses, with ice melt being the main factor respon-

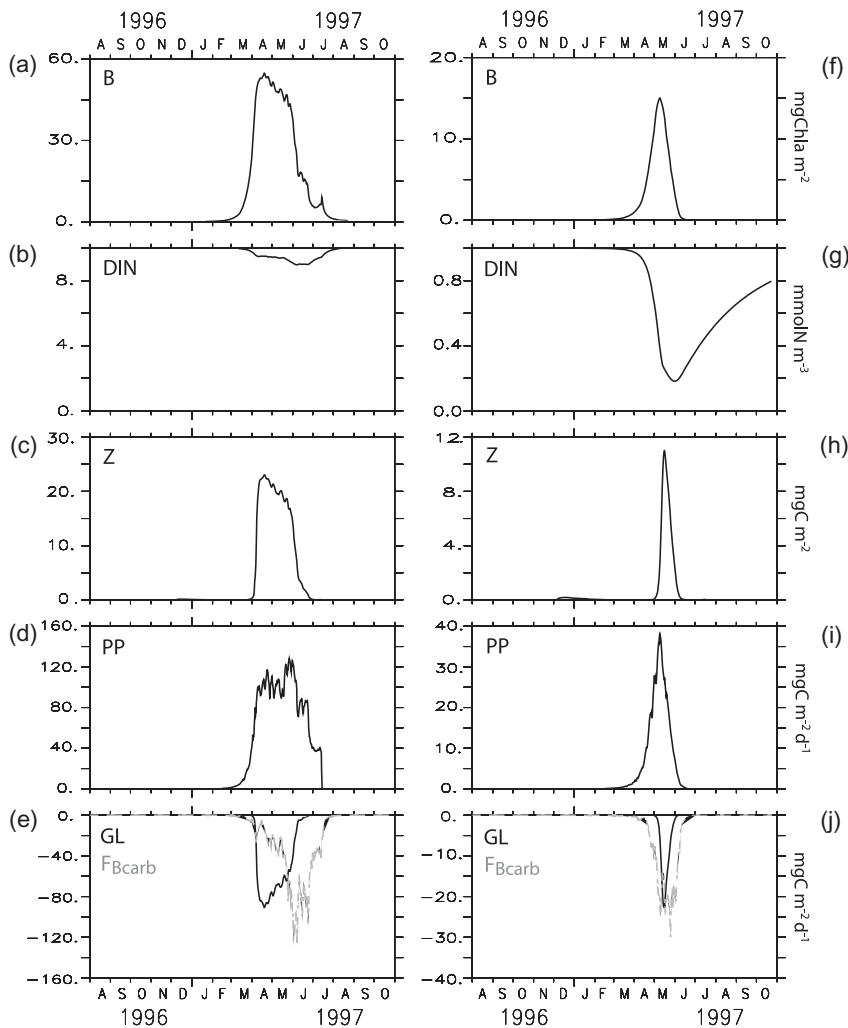


Fig. 3 Results of the set-up simulations for two scenarios of nutrient conditions. (a–e) HN scenario, i.e., high nutrient availability and high turbulent mixing; (f–j) LN scenario, i.e., low nutrient availability and low turbulent mixing. (a, f) Ice algal biomass (*B*); (b, g) dissolved inorganic nitrogen concentration in the upper water layer (*DIN*); (c, h) ice-faunal biomass (*Z*); (d, i) ice algal production (*PP*); (e, j) loss rates due to grazing (*GL*; solid line) and sea-ice melt (*F_{Bcarb}*; grey dashed line).

sible for the bloom decline in late spring. The simulated ice-associated fauna reaches, in mid-April, a maximum biomass and production of 22 mg C m^{-2} and ca. $80 \text{ mg C m}^{-2} \text{ day}^{-1}$, respectively. Under this scenario, the maximum loss rate of ice algae as a result of ice melt ($125 \text{ mg C m}^{-2} \text{ day}^{-1}$) occurs in early June.

Compared with the HN scenario, the simulated ice algal bloom occurs 1 month later under the LN scenario (Fig. 3). The bloom is significantly less intense (maximal biomass of ca. $15 \text{ mg Chla m}^{-2}$ and primary production of $37 \text{ mg C m}^{-2} \text{ day}^{-1}$), and is of shorter duration (from early April to mid-June), compared with the HN scenario. This is mainly because of the effect of nutrient limitation on the growth rate, and of photoacclimation processes on ice algal photosynthetic activity under the LN scenario until April–May (Fig. 4). Changes in *Chla/C* ratios (which is used as an indicator of the physiological acclimation of the cells to change in irradiance), E_k parameters, and limitation terms for light (Lim_E) and nutrients (Lim_N)

under both LN and HN scenarios are shown in Fig. 4. *Chla/C* ratios are higher under the HN scenario (0.05–0.092) than under the LN scenario (0.03–0.062). This indicates that ice algae respond to environmental constraints by changing their cellular *Chla* content. At equal light intensities (PAR_{subice}), the LN scenario shows a more elevated E_k , delaying the beginning of production by about 2–3 weeks (Fig. 3). In the HN scenario, light limitation (Lim_E) rapidly decreases from mid-May, and there is no nutrient limitation (Lim_N). In contrast, light limitation lasts longer and nutrient limitation becomes severe starting in May under the LN scenario. As both Lim_N and Lim_E act together in a multiplicative way in the growth rate equation (see Eqn. 1 in Table 2), the effect is then stronger for the LN scenario. The lower ice algal biomass produced by the LN scenario leads to an ice faunal biomass of only 11 mg C m^{-2} , representing half of the faunal stock estimated for the HN scenario. The loss of ice algal biomass because of ice melt in the LN scenario is

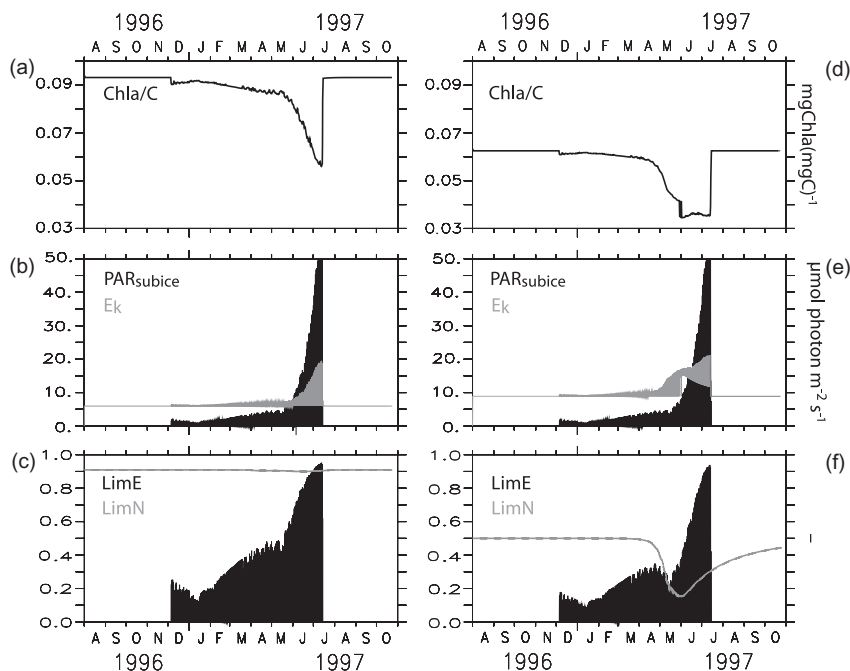


Fig. 4 Results of the set-up simulations for two scenarios of nutrient conditions. (a–c) HN scenario, i.e., high nutrient availability and high turbulent mixing; (d–f) LN scenario, i.e., low nutrient availability and low turbulent mixing. (a, c) Chlorophyll *a*/C ratio; (b, e) sub-ice photosynthetically available radiation (PAR_{subice}) and photoacclimation parameter (E_k) superimposed; (c, f) light ($LimE$) and nutrient ($LimN$) limitation terms.

always higher than that due to grazing: it starts earlier and lasts longer, but has a similar intensity (ca. $20 \text{ mg C m}^{-2} \text{ day}^{-1}$).

These set-up simulations, although idealized, produce an ice algal biomass and bloom timing in agreement with previous observations under similar conditions (e.g., Gosselin et al. 1985; Runge et al. 1991; Kudoh 1995; Suzuki et al. 1997; Mock & Gradinger 1999; Fortier et al. 2002; Lavoie et al. 2005; Jin et al. 2006). Estimates of the ice-associated faunal biomass are far scarcer than those for ice algae, leading to some uncertainties in the results from the model. Nevertheless, the simulated values under the HN scenario are consistent with faunal biomass estimates ranging from 0 to 20 mg C m^{-2} at the bottom of the sea ice of northern Baffin Bay (Nozais et al. 2001). Furthermore, under both scenarios, ice fauna can graze between 0.2 and 4.1% of the bottom ice algal production, and between 0.05 and 0.68% of the ice algal standing stock. Similar values were reported for bottom-ice meiofauna (0.55–5.7 and 0.05–0.92% of the production and standing stock, respectively) by Nozais et al. (2001), and for under-ice amphipods (1.1–2.6% of the algal standing stock) by Werner (1997).

We performed another set of sensitivity simulations on snow thickness (not shown), which is an important factor affecting the light limitation of ice algae. Snow thickness is highly variable in the sea-ice–ocean model, both in time and space, so that spatially averaged values are extremely low (less than 1 cm). Hence, we tested its effect with an idealized snow thickness forcing equivalent to 5

and 10% of the sea-ice thickness layer imposed over the whole simulation period. In response to increased albedo and light attenuation, even low snow thicknesses (< 10 cm) had a dramatic effect on the simulated ice algal biomass, which is reduced by more than 90% in both scenarios, whereas the timing and extent of production are delayed and strongly reduced, respectively. Even though these simulations are not realistic, a strong decrease of ice algal biomass under significant snow thickness has already been observed by several authors (e.g., Gradinger et al. 1991; Arrigo & Sullivan 1994; Lavoie et al. 2005; Riedel et al. 2007). All our set-up simulations described above indicate that light availability is the main factor affecting the timing and duration of the simulated ice algal dynamics.

The spatially averaged results of the coupled simulation (Fig. 5) give a situation intermediate to those of the two previous distinct scenarios, indicating that the general behaviour of the ice alga model is conserved in the 3D model. The simulated bloom period lasts from early March until the end of June, with a maximal chlorophyll concentration (ca. $20 \text{ mg Chla m}^{-2}$) occurring during the third week of April. These lower Chla concentrations compared with the HN scenario may result from the strong variability of the Chla/C ratio over the domain. Simulated DIN concentrations in their upper water layer reach the mean maximum in March–April (ca. $3.5 \text{ mmol N m}^{-3}$), in response to autumn and winter mixing. Thereafter, DIN concentrations remain above 1 mmol N m^{-3} , even during the ice algal bloom. Wind

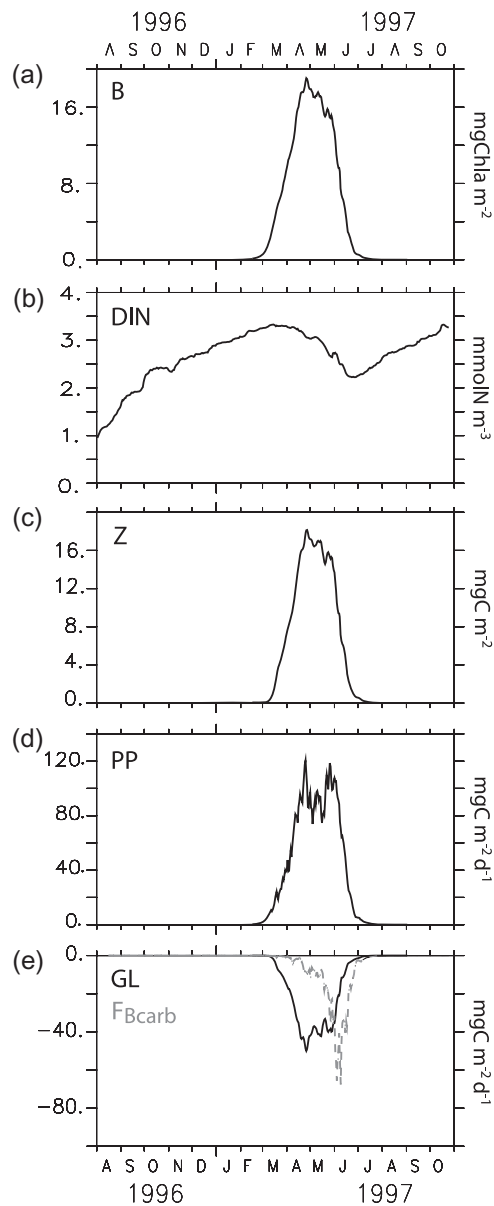


Fig. 5 Spatially averaged results of the ice algal production model for the whole Hudson Bay system (including Hudson Bay, James Bay, Foxe Basin and Hudson Strait) for coupled simulations. (a) Ice algal biomass (*B*); (b) dissolved inorganic nitrogen concentration in the upper water layer (*DIN*); (c) ice-faunal biomass (*Z*); (d) ice algal production (*PP*); (e) loss rates due to grazing (*GL*; solid line) and sea-ice melt (*F_{Bcarb}*; grey dashed line).

mixing in summer and early autumn allows nutrient replenishment of the ice-free surface waters. Simulated faunal biomass follows the same pattern as ice algal biomass, with a mean maximum value (16 mg C m^{-2}) occurring at the end of April. The increase in ice faunal biomass starts about 2 weeks later compared with that of the ice algae. This is consistent with results from the set-up simulations (Fig. 3). Simulated mean primary and

secondary productions reach ca. $120 \text{ mg C m}^{-2} \text{ day}^{-1}$ and $50 \text{ mg C m}^{-2} \text{ day}^{-1}$, respectively. The simulated sinking of algae because of ice melt starts from mid-April, with a sharp increase from mid-May to early June. Overall, these ice algal and faunal biomasses, productions and timings correspond to the HN scenario, and suggest a slight nutrient limitation and a regulation of the primary production by grazers until the late spring melting rate induces the release of ice algae into the water column.

Spatial variability of the simulated seasonal cycle over the Hudson Bay system

The large spatial variability of the ice algal production is mainly driven by the spatial heterogeneity of the ice conditions (Fig. 6), as this is the major factor affecting light conditions in the HBS as a whole. A detailed description of the simulated ice-cover dynamics for this simulation is given in Saucier et al. (2004), and here we only summarize the main patterns. The ice cover increases rapidly in late autumn–early winter in the HBS, mainly because of thermodynamic growth, and is almost complete by the end of December. Later in the season, thermodynamic sea-ice growth is confined to western Hudson Bay, western Foxe Basin and along the south shore of Hudson Strait, whereas mechanical ridging dominates in southern Hudson Bay and eastern Foxe Basin, where the maximum sea-ice thicknesses are found in late winter (see Saucier et al. 2004: fig. 13). This accumulation of ice in the eastern Hudson Bay is the result of general cyclonic circulation and eastward wind-driven circulation prevailing throughout wintertime. As a result, ice conditions in March (Fig. 6) reveal a large area of low ice thickness ($<1 \text{ m}$) in western Hudson Bay and eastern Hudson Strait, including Ungava Bay, that contrast with higher ($2\text{--}4 \text{ m}$) ice thicknesses in the eastern Hudson Bay and Foxe Basin. This situation remains until spring when the maximum ice thickness area shifts along the south-west shore of Hudson Bay (see Fig. 6 for April).

Ice melt begins in early May in nearshore areas of the north-west Hudson Bay and Hudson Strait, and increases over the whole system in mid-June. At the end of July, sea ice covers less than 10% of the HBS, and is mainly confined to Foxe Basin and southern Hudson Bay, with thicknesses of $1.5\text{--}2.0 \text{ m}$ and $0.5\text{--}1.0 \text{ m}$, respectively. A notable and important feature is the early opening of the ice cover near the north-west coast of Hudson Bay in February–March, which is the result of wind-driven transport of sea ice causing the formation of a quasi-permanent latent heat polynya in this region. In contrast, the early opening in eastern Hudson Strait in February is instead the result of tidally induced mixing (LeBlond et al. 1981; Straneo & Saucier 2008), and is therefore a

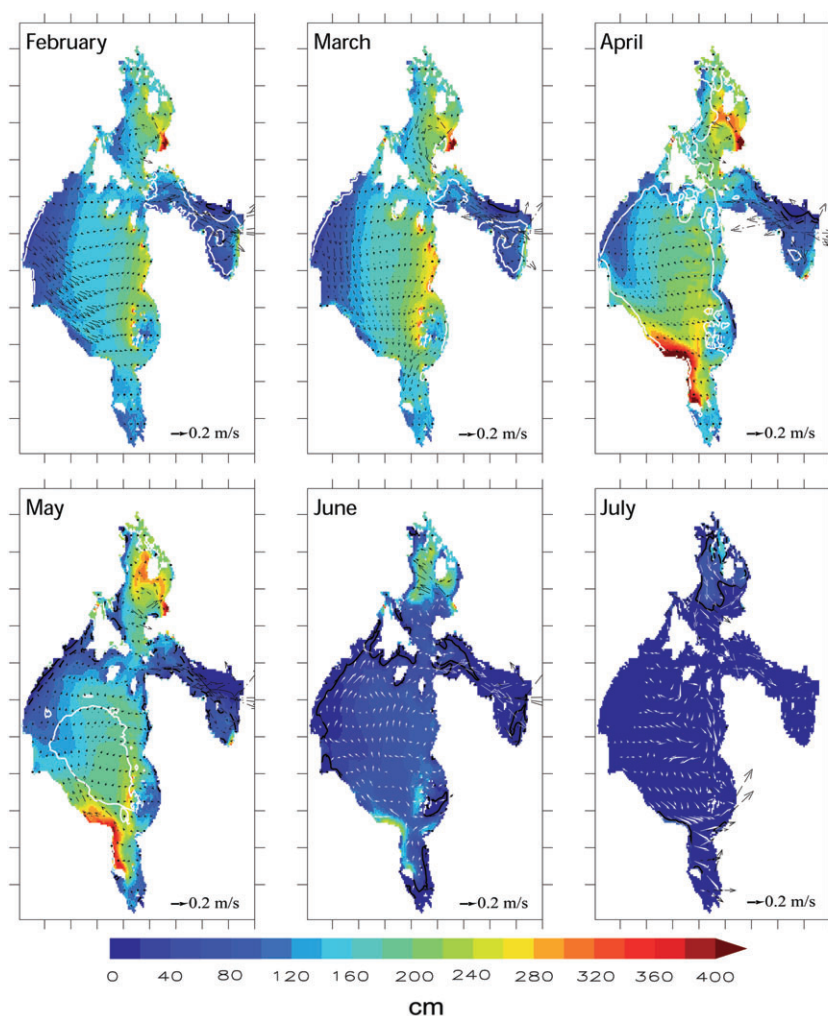


Fig. 6 Monthly averaged sea-ice thickness for the coupled simulation from February to July 1997. Sea-ice horizontal transport velocity (m s^{-1}) and sea-ice coverage (10%, black line; 50%, dashed black line; 90%, white line) are superimposed on each graph.

sensible heat polynya. Saucier et al. (2004) showed that this simulated seasonal ice pattern and its spatial variability in HBS were able to reproduce observations from the sea-ice charts produced by the Canadian Ice Service.

The effects of this spatial heterogeneity of ice conditions on ice algal dynamics (biomass and production) are shown in Figs. 7, 8. Significant ice algal accumulation first appears in the south-west part of Hudson Bay, close to the Nelson River, in early March (Fig. 7). The bloom then extends north into the bay, along the western marginal ice zone, until May. At the end of this period, an ice algal bloom between 30 and 60 mg Chla m^{-2} occurs over most of the HBS where ice thickness does not exceed 2 m (Fig. 6). Simulated ice algal primary production rates (Fig. 8) in the higher biomass areas (i.e., western Hudson Bay, Foxe Basin and southern Hudson Strait, including Ungava Bay) are over 300 $\text{mg C m}^{-2} \text{ day}^{-1}$. Later in June, the ice algal biomass distribution follows the ice retreat from west to east, but with very low ice algal biomass and

production (<15 mg Chla m^{-2} and <40 $\text{mg C m}^{-2} \text{ day}^{-1}$, respectively) in most of the system, except for the northernmost part of Foxe Basin, where residual sea ice allows late ice algal growth (Figs. 7, 8). Low DIN availability (0–1 mmol N m^{-3}) in the upper water layer occurs in areas influenced by freshwater, especially in James Bay and eastern Hudson Bay (Fig. 9). The freshwater influence combines with high ice thickness to strongly limit ice algal production, which cannot occur at significant levels before the rapid ice melt in June–July in these areas. In all other areas, the ice algal bloom only partially depletes nutrients in the upper water layer. With minimum values of ca. 2–3 mmol N m^{-3} in June after uptake by ice algae in central and western Hudson Bay, nutrient limitation reduced ice algal production by 25–40% just before the release of ice algae into the water column as a result of ice melt.

We extracted high-frequency time series for selected stations along a north-west–south-east transect

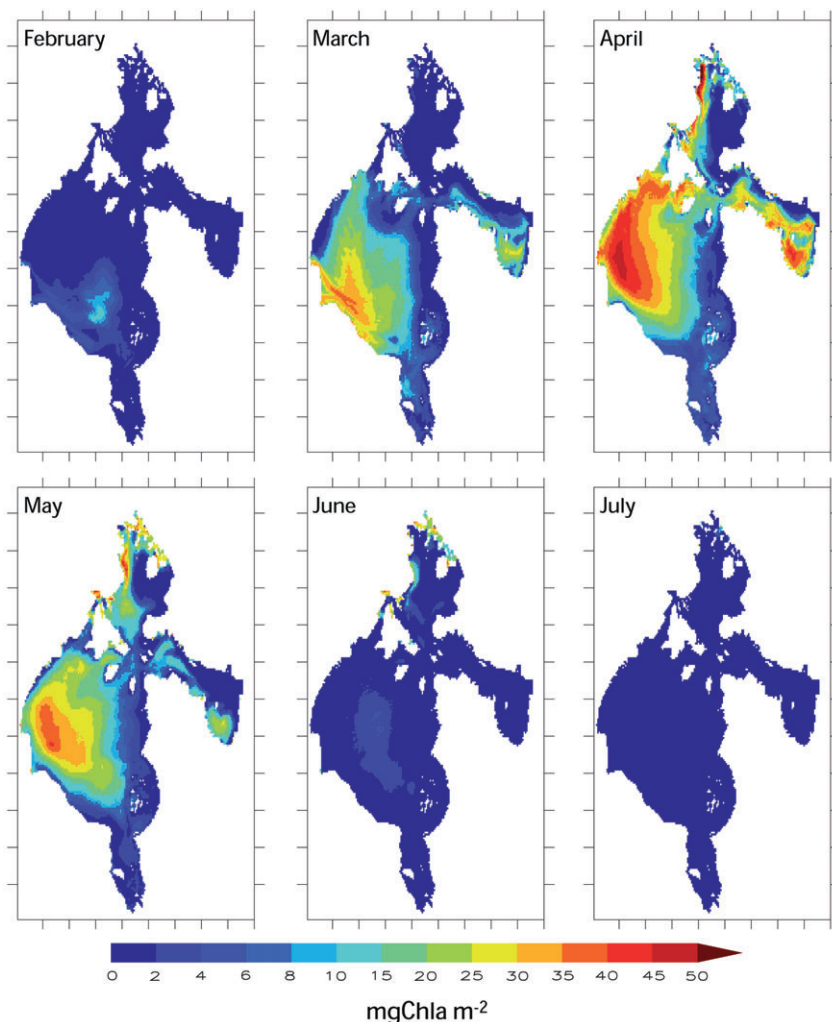


Fig. 7 Monthly averaged ice algal biomass per m^2 of sea ice for the coupled simulation from February to July 1997.

(Fig. 10a–e) in Hudson Bay, and along a south–north transect (Fig. 10f–j) from James Bay to Foxe Basin to better examine the temporal trends (see Fig. 1 for the station locations). Station 3 in eastern Hudson Bay is presented in both panels to highlight the strong biophysical variability between both transects. Stations from Hudson Bay are characterized by maximal ice thicknesses ranging from 1 m (station 1 in western Hudson Bay) to 2.2 m (stations 2 and 3 in central and eastern Hudson Bay, respectively). Stations 1 and 2 show high ice algal biomasses, and production reaching $70\text{--}130 \text{ mg Chla m}^{-2}$ and $240\text{--}575 \text{ mg C m}^{-2} \text{ day}^{-1}$, respectively, between April and June. Nutrient depletion at stations 1 and 2 occurs at the end of May and persists until ice breakup in June, when water column mixing replenishes the upper layer. The time series of station 3 illustrates the thicker ice cover and low nutrient availability ($<1.5 \text{ mmol N m}^{-3}$) affecting the primary production (max. $30 \text{ mg C m}^{-2} \text{ day}^{-1}$) and biomass accumulation ($<20 \text{ mg Chla m}^{-2}$) of ice algae. For

stations along the south–north transect, the ice thicknesses varied between 1.5 and 2.8 m, which largely limits light availability at the ice–water interface. At station 5 in Foxe Basin, a significant ice algal biomass accumulation and production (up to $40 \text{ mg Chla m}^{-2}$, and to $100 \text{ mg C m}^{-2} \text{ day}^{-1}$, respectively) is not seen before early June, i.e., 2 months later than at station 1, and despite high nutrient availability ($>5 \text{ mmol N m}^{-3}$). Station 4 (James Bay) shows similar patterns to station 3, with low ice algal biomasses and daily integrated production ($10 \text{ mg Chla m}^{-2}$ and $20 \text{ mg C m}^{-2} \text{ day}^{-1}$, respectively), associated with the very low nutrient concentrations ($<1 \text{ mmol N m}^{-3}$) despite a moderate ice thickness ($\leq 1.5 \text{ m}$). Grazing also affects the biomass of ice algae during the bloom period (Fig. 10e,j). This is the case for stations with higher ice algal production (stations 1 and 2), whereas grazing has little effect on the less productive stations (mainly stations 3 and 4). Ultimately, the ice-melt process ended the production period in every case by

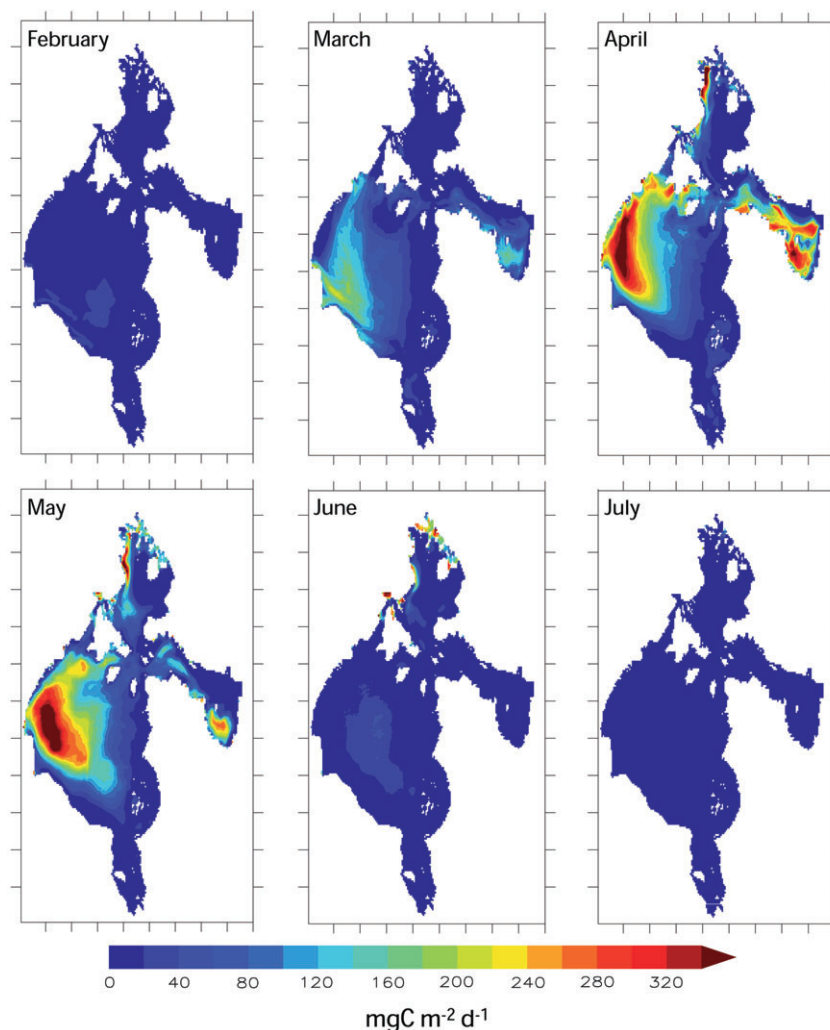


Fig. 8 Monthly averaged ice algal production for the coupled simulation from February to July 1997.

inducing the release of ice algae into the water column. This is particularly evident in Foxe Basin (station 5), where ice melt occurs rapidly in early June, hence shortly after the start of the ice algal bloom, which ends abruptly before July.

The model did not exhibit a significant response of ice algal production to changes in snow thickness. This is because of the rapid snow/ice compaction rate in the ice–snow model of Saucier et al. (2004), which prevents significant snow accumulation. Figure 10 shows that the simulated snow cover thickness is generally lower than 4–5 cm, even for high-frequency time series. The effect of snow cover on ice algal production is therefore spatially under-represented in our model. The sharp decrease in ice algal biomass and production that appears at station 3 in early April is likely to be associated with pack ice transport by currents, as there was no change in snow thickness nor in ice melt at this time of the year.

Our results from the five high time-frequency stations confirm and strengthen the primary role of sea-ice dynamics and nutrient availability on the high spatiotemporal variability of ice algal production and biomass in the HBS (Fig. 3).

Simulated release of the organic matter produced by the sea-ice ecosystem and its potential fate in the ocean

Figure 11 shows the fate of POM produced by the sea-ice ecosystem when released into the water column along a west–east transect across the Hudson Bay (see dashed line in Fig. 1). POM in the water column results from losses of ice algae and fauna by ice melt, and of fauna by mortality. Significant POM concentrations are first observed in the upper water column in the western part of the bay in April (Fig. 11), when the biomass of ice algae and fauna are maximal (Figs. 5, 7). Maximum POM values in

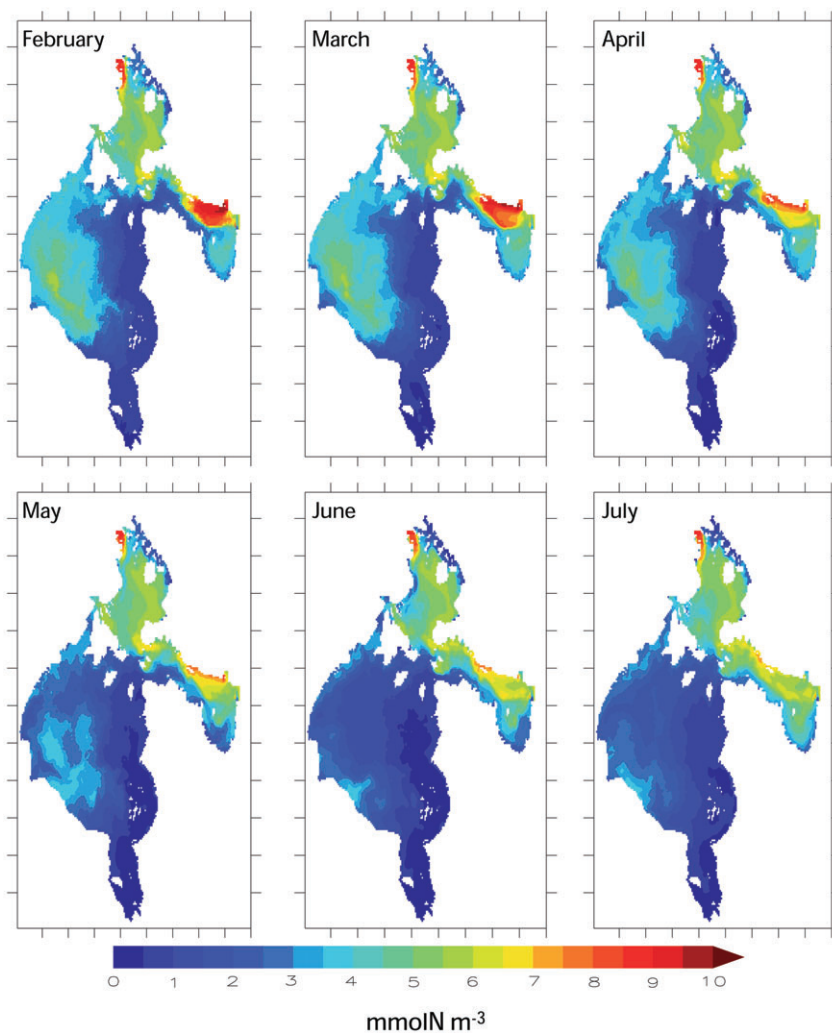


Fig. 9 Monthly averaged dissolved inorganic nitrogen concentration in the upper water layer for the coupled simulation from February to July 1997.

May–June logically correspond in time with sea-ice melt, and in space with the west–east gradient of ice algal productivity. In July, most of the POM has reached mid-depth (40–160 m) in the deeper part of the bay or the bottom in the shallower western area. The near-complete downward sinking of the POM to the deeper layers (>150 m) is achieved in August. Maximum POM concentrations in the high ice algal productivity area are ca. $0.33 \text{ mmol N m}^{-3}$, which corresponds to 26 mg C m^{-3} , assuming freshly produced organic matter and a Redfield C/N molar ratio of 6.65. Near-bottom values in August in the central and deeper part of the bay are ca. $0.16 \text{ mmol N m}^{-3}$, representing 12.8 mg C m^{-3} .

Figure 12 illustrates the seasonal fate of depth-integrated POM concentrations on the regional scale from March to August. The higher depth-integrated values are first found in May–June in the western more productive areas (i.e., in southern Hudson Strait and Ungava Bay, as well as in Foxe Basin). This figure also shows POM spread-

ing through the system, driven by the general cyclonic circulation. Simulated sedimentation rates vary nonlinearly with POM concentration, so that POM residence time in the surface layers is shorter (by about a month) than at intermediate depths (2–3 months). The spreading of POM in low productivity areas is in part limited by the bathymetry of the basin, with the shallower areas east of Hudson Bay and Foxe Basin being less affected by POM transport. The formation of a cyclonic gyre between 80 and 150 m depth in the middle–western part of Hudson Bay in June–July (also observed by Saucier et al. 2004) implies a local retention of suspended material in this area, with an increased POM concentration.

Figure 13 shows the ice algal production, the release flux of ice algae and fauna in the upper water layer, and the accumulated POM at the seafloor integrated over the year 1997. All these rates are expressed per unit of square metres of ocean. The simulated annual primary production ranges from less than $1 \text{ g C m}^{-2} \text{ year}^{-1}$ (in the eastern

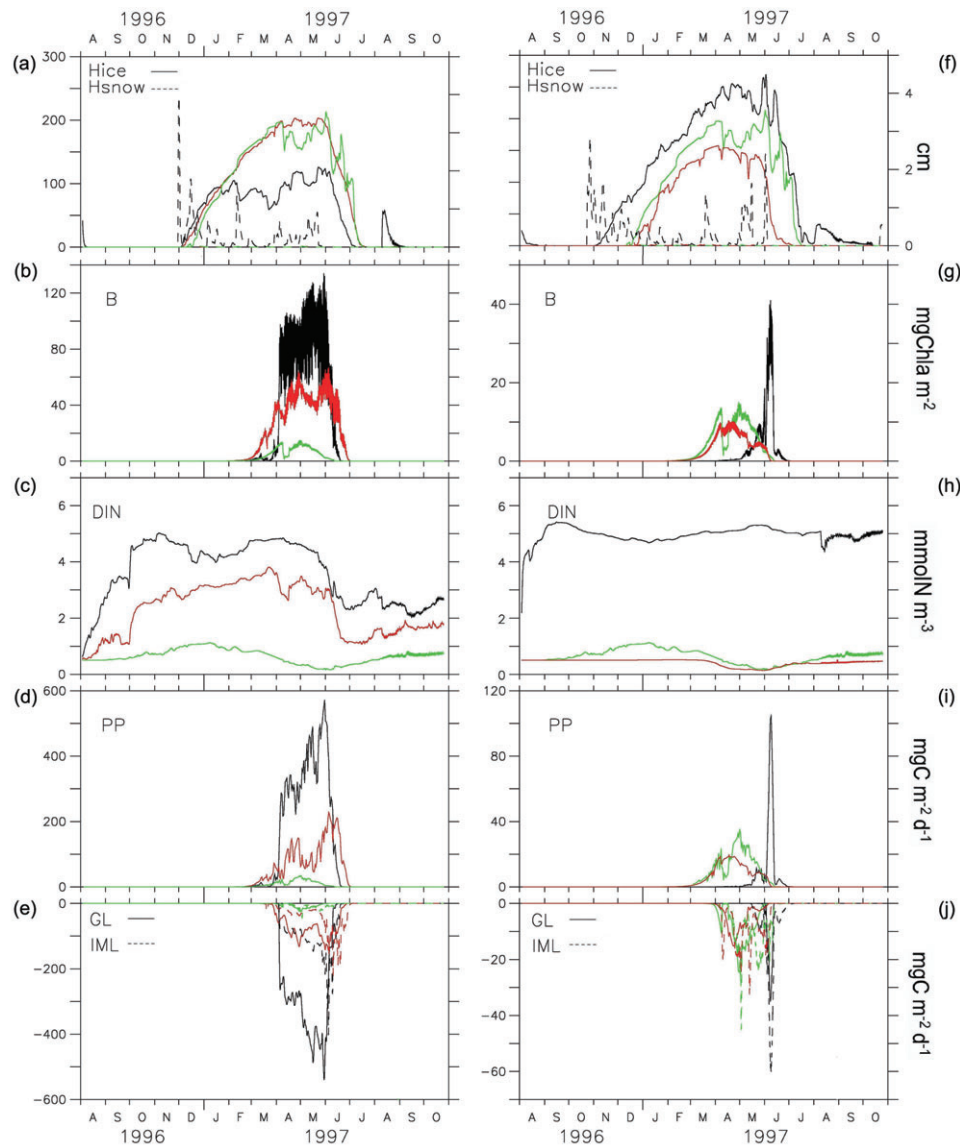


Fig. 10 High-frequency (10 min) time series for stations located along a north-west–south-east transect in Hudson Bay. (a–e) Station 1 in western Hudson Bay (black curve), station 2 in central Hudson Bay (red curve) and station 3 in eastern Hudson Bay (green curve). (f–j) Along a south–north transect: station 4 in James Bay (red curve), station 3 in eastern Hudson Bay (green curve) and station 5 in Foxe Basin (black curve). (See station locations in Fig. 1.) Station 3 is intentionally presented in both panels for comparisons. (a, f) Sea-ice and snow thicknesses (H_{ice} , H_{snow}); (b, g) ice algal biomass (B); (c, h) dissolved inorganic nitrogen concentration in the upper water layer (DIN); (d, i) ice algal production (PP); (e, j) losses due to grazing (GL ; solid line) and sea-ice melt (F_{Bcarb} ; grey dashed line).

part of the bay and Foxe Basin) to $20\text{--}25\text{ g C m}^{-2}\text{ year}^{-1}$ (in the western part of the bay, north-west Foxe Basin and Ungava Bay). The simulated sinking flux gives an estimate of the ice-produced POM that can reach the seafloor. Similar to ice algal production and POM release flux, the maximum fluxes at the seafloor (ca. $0.6\text{ g C m}^{-2}\text{ day}^{-1}$) are observed in the western Hudson Bay, western Foxe Basin and Ungava Bay. The fraction of ice algal production that reaches the seafloor ranges from 1 to 10%. At the end of the summer, in August 1997, more

than 90% of the POM release from the sea ice remains in the water column. This calculation assumes that the POM was not subject to transformation (no utilization nor regeneration) in the water column.

Discussion

Understanding the dynamics of ice algae and their fate in a warming Arctic is a pertinent issue given the rapidity of environmental changes (Carmack et al. 2006; Wassmann

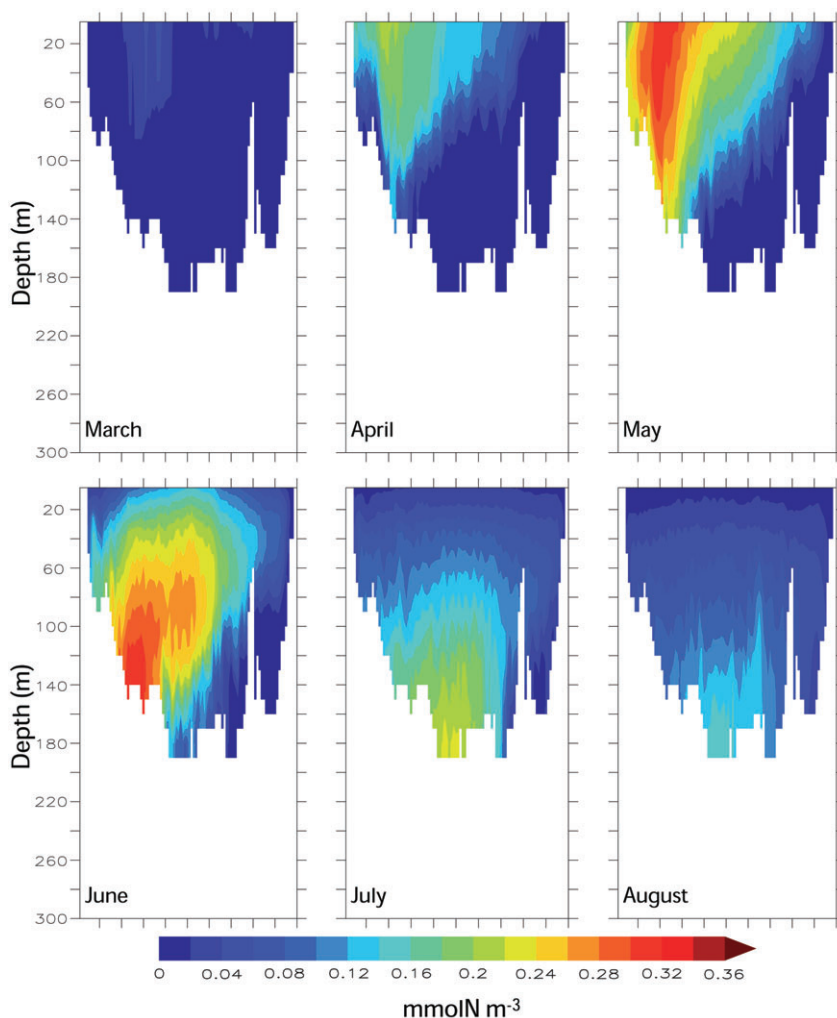


Fig. 11 Monthly averaged vertical distributions of the particulate organic matter (POM) concentration along longitudinal transect across Hudson Bay (see dashed line in Fig. 1) for the coupled simulation from March to August 1997.

et al. 2008) that will strongly affect their habitat (e.g., Smetacek & Nicol 2005). One challenge, in addition to the harsh weather and remoteness that characterize polar regions, is the large range of spatial scales for physical and biological processes involved. On the one hand, the biology of ice algae strongly depends on ice dynamics, which involve small-scale (10^{-2} – 10^{-3} m) processes such as brine channel formation and distribution that influence the transmission of irradiance at the bottom ice (Le Fèvre et al. 1998; Mock & Gradinger 2000), as well as nutrient (Cota et al. 1987; Mock & Gradinger 2000) and space (Krembs et al. 2000; Mundy et al. 2007) availability. On the other hand, ice algal productivity and distribution are greatly affected by ice and snow thicknesses (through their effect on light availability within and at the bottom of the sea ice), which are influenced by meso- to synoptic-scale processes such as meteorological conditions (e.g., precipitation), wind-driven current transport and ridging (Arrigo 2003; Eicken 2003). Numerical mod-

elling tools such as we present here can help to increase our understanding of ice algal dynamics at meso- to synoptic scales, but cannot fully capture all processes given the large spatial scales involved. It was necessary to simplify the small-scale physical processes driving the ice algal habitat in the present study.

The sea-ice ecosystem model uses the cell-averaged ice conditions (snow and ice thicknesses and ice coverage), and is not implemented per se in the multi-category, two-layer ice model. The transport of sea ice is made with a conservative advection scheme using cell-averaged sea-ice velocities independently of the mechanical redistribution of sea ice resulting from ridging, which would imply some ice algal mixing from the bottom ice layer inside the ice (Hegseth & von Quillfeldt 2002). The present ice alga model does not take into account the ice algal stock within the entire ice column, which would require a fine-scale depth resolution of the sea ice (e.g., Arrigo et al. 1993; Lavoie et al. 2005) not allowed with

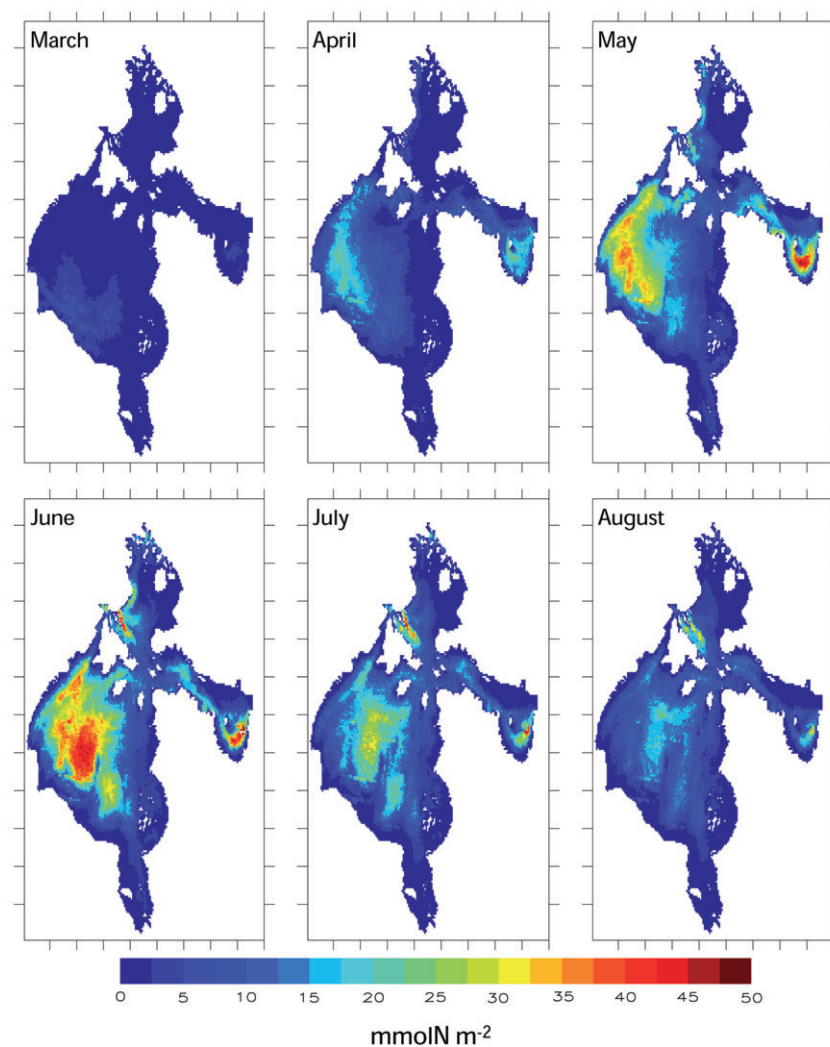


Fig. 12 Monthly averaged depth-integrated particulate organic matter (POM) concentration in the Hudson Bay system for the coupled simulation from March to August 1997.

the present sea-ice model. Previous observations in the Arctic suggest that the within-ice algal stock may be of limited importance in first-year sea ice (Booth 1984; Gradinger et al. 1991; Arrigo 2003). Similarly, as the dynamics of the surface melt ponds are generally not well understood, this component was not included in the present 3D ice alga model. The contribution of these surface meltwater ponds to the global ice productivity is likely to be low compared with layers at the base of the sea ice (Gradinger 1996). Both accretion and ridging are nevertheless included in the multi-category sea-ice model, affecting ice thickness and bottom-ice light availability, and therefore the simulated ice algal dynamics. This effect is particularly important in eastern Foxe Basin and south-eastern Hudson Bay, where mechanical sea-ice growth may be of the same order of magnitude or greater than the thermodynamic one in spring (see Saucier et al. 2004: fig. 13).

Moreover, the model does not consider the thermodynamics of the bottom ice layer colonized by algae. The structure of this layer, i.e., the geometry and distribution of brine channels at the near-bottom ice interface, determines the surface and volume available for biomass development and accumulation. The initial colonization by algae and the associated heterotrophic organisms of the semi-solid ice matrix are thought to be mainly the result of the entrapment of open-water organisms during early sea-ice growth (Gradinger & Ikävalko 1998; Krembs et al. 2002; von Quillfeldt et al. 2003; Rozanska et al. 2008). The subsequent survival of organisms and species selection may depend on the evolution of the ice structure (Lizotte 2001). Sea-ice colonization was formulated here with a simple settlement rate used for a well-settled ice sheet (>20 cm), but decreases as the ice thickens in winter. This was primarily designed as a way to limit colonization to the early winter season, as colonization

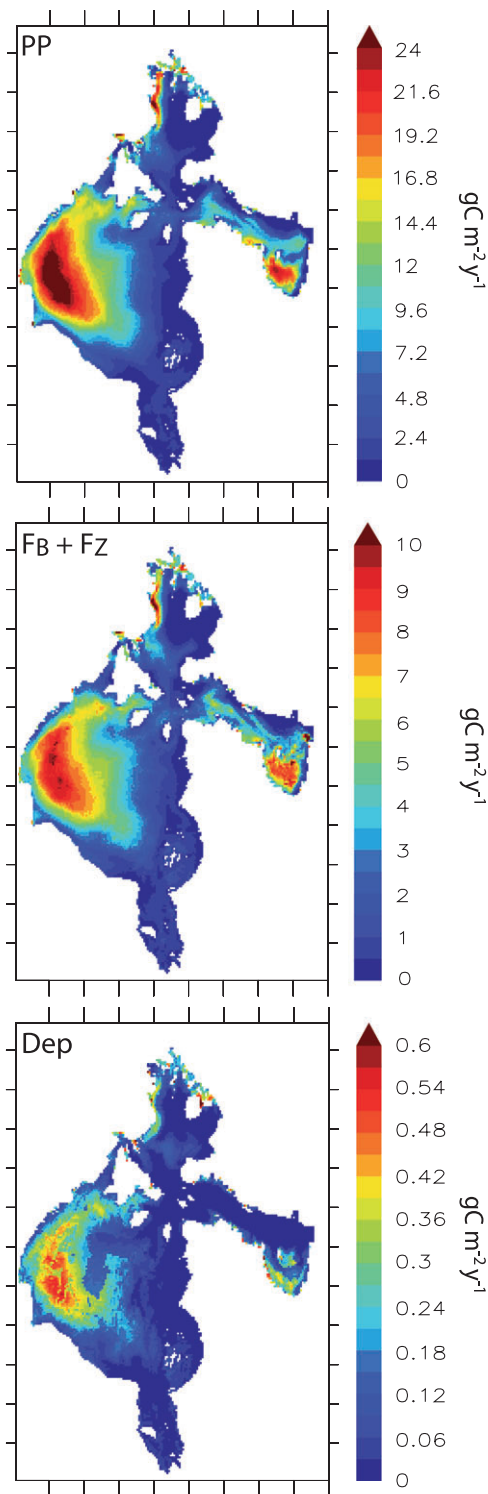


Fig. 13 Annually integrated ice algal production (PP), total release flux of ice algae and ice fauna into the water column ($F_B + F_Z$) and accumulated particulate organic matter (POM) at the seafloor (Dep) in the Hudson Bay system. The data were integrated for the period between January and October 1997.

processes for increasing sea-ice thickness during winter are considered to be minor (Lizotte 2001). The assumption of a well-settled ice sheet can be debatable given the dominant role of very early ice formation processes for the colonization of sea ice: mainly suspension freezing that may “sample” the upper water column (Gradinger & Ikävalko 1998; Krembs et al. 2002) for both inorganic and living particles. Nevertheless, the duration of early ice formation is short enough compared with the seasonal ice cycle that these processes may be assumed as implicit in our model.

The thermodynamics and structure of the bottom ice layer also affect nutrient availability for ice algae (Lytle & Ackley 1996). The within-ice nutrient content first depends on the nutrient concentration of the frozen sea water and later on brine exclusion, this latter process being driven by the thermodynamics of the sea ice. This internal source is often limited in the Arctic, and the underlying upper-ocean mixed layer is the main source of nutrients during the late spring ice algal bloom in this region (e.g., Horner & Schrader 1982; Maestrini et al. 1986; Cota et al. 1987). It has been shown in several locations that the nutrient flux toward the ice–ocean interface depends on the hydrodynamics of the underlying seawater, with tidally induced mixing being a major forcing on arctic shelves (Gosselin et al. 1985; Demers et al. 1989; Lavoie et al. 2005). The combined effect of processes related to ice thermodynamics and ocean hydrodynamics on nutrient fluxes between sea ice and the ocean is not straightforward to formulate given the different spatial scales involved. A simpler formulation, used by Lavoie et al. (2005), assumes molecular diffusion through a molecular sublayer that varies with the kinematic viscosity of seawater and friction velocity, with the latter varying with tidal currents. Nishi & Tabeta (2005, 2007) developed a more sophisticated boundary layer formulation forced by the thermodynamics of ice growth/melting rates and empirical formulations for brine volume outflow. Arrigo et al. (1993) used a similar approach that also included the platelet ice layer that is characteristic of Antarctic ice by applying a bulk material transport coefficient. Whereas any of these formulations could have been used in our model, it can be argued that the high tidal forcing in the HBS (Saucier et al. 2004) would ensure high sea-ice–ocean nutrient fluxes. These fluxes are then assumed to instantaneously supply the ice algal nutrient demand. Moreover, such semi-empirical formulations may need a sensitivity analysis for the parameters used; this is a time-consuming task in a 3D modelling experiment. Indeed, the present coupled simulation shows a marked effect of nutrient limitation in the eastern Hudson Bay affected by freshwater run-off with low DIN concentrations (e.g., Hudon et al. 1996), leading

to very low simulated biomasses and productions of ice algae. A more refined formulation of the ice–ocean nutrient flux would only strengthen this feature.

The only exception concerning these small-scale related simplifications is the effect of bottom ice melt on the sloughing (release) of ice algae, which is a major process leading to the decline and termination of ice algal blooms (Granskog 1999). The melt-driven sloughing rates for ice algae and the associated grazers are forced by the thermodynamics of bottom-ice melting calculated by the sea-ice model. Although formulated with a bulk representation, this allows the model to keep melt-driven loss rates consistent with the simulated ice dynamics, particularly during the bloom decline. Lateral melting is generally far lower than bottom-ice melting in our simulation (not shown), and was therefore not considered in the sea-ice ecosystem melting loss term. The same assumption was made for bottom melting resulting from the conversion of solar radiation into heat by ice algae: this process can induce a loss of the algal habitat as well as ice algal release into the water column (Zeebe et al. 1996). As this results in only a small fraction of the total bottom melting loss, it was not included in our model.

Some ecological assumptions have also been made to keep the model simple and efficient, with the intention of coupling this model with a water column planktonic ecosystem model in the future. The first assumption was to ignore the biodiversity of the sea-ice ecosystem. The ice algal compartment is generally occupied by diatoms, dinoflagellates and other eukaryote taxa, as well as cyanobacteria (e.g., Lizotte 2003). As soon as algae from the water column are trapped in the ice, a natural selection occurs, favouring better-adapted species and then limiting their number (Horner & Schrader 1982). Among these adapted species, diatoms are good competitors and are of major importance during ice algal blooms in polar environments (Poulin & Cardinal 1982, 1983; Ikävalko & Thomsen 1997; Rozanska et al. 2009). We acknowledge that our model does not take into account photophysiological differences between ice algal species (Hegseth 1992; Cota & Smith 1991b; McMinn et al. 2007), but it reflects the response of the total community during their growth season (Kirst & Wiencke 1995). The situation is also quite complex for the ice faunal compartment in Arctic regions because of a relatively high biodiversity. Turbellarians, young stages of harparcticoid copepods, nematodes and rotifers are all found in the ice (Schnack-Schiel 2003). Among these taxa, late stages of the calanoid copepods *Pseudocalanus* sp. and *Calanus glacialis* inhabiting the upper water column are known to graze actively on ice algae (Conover et al. 1986; Runge & Ingram 1988). At this stage of the development of the model, we took into consideration the grazing compart-

ment present at the bottom of the sea ice, which is composed of different taxa belonging to microfauna and meiofauna (Schnack-Schiel 2003). An improvement of the model would then be to take into account grazing of ice algae by ice macrofauna (Schnack-Schiel 2003), such as ice amphipods and under-ice zooplankton (Runge & Ingram 1988; Conover & Huntley 1991), such as copepods and other zooplankton grazers.

Bacterial communities are plentiful in the sea-ice ecosystem, making up the most abundant heterotroph in the ice (e.g., Lizotte 2003; Kaartokallio 2004), and allowing nutrient regeneration through an active microbial loop (e.g., Laurion et al. 1995; Kaartokallio 2001; Riedel et al. 2007). No bacterial compartment has been included in this model, but the regeneration process is implicit in the way the non-assimilated part of grazed ice algae is instantaneously regenerated in the model. The last ecological assumption concerns the choice of limiting nutrients for ice algal growth in the bottom-ice layer. Many studies indicate that ice algal growth is limited by dissolved nitrogen (Grainger et al. 1977; Maestrini et al. 1986; Smith et al. 1997) or by dissolved silicon (Cota & Sullivan 1990; Gosselin et al. 1990; Smith et al. 1990). The strong spatial variability and the abrupt change of local chemical conditions in HBS (coastal–offshore gradients), in part resulting from the strong influence of freshwater run-off, could strongly influence which nutrient is the most limiting. In the present model, we focus on the regulation and supply of dissolved inorganic nitrogen and its effects on ice algal growth. Again, this part of the model is simplified with the idea that it will later be coupled with a planktonic ecosystem model.

These ecological assumptions are similar to those often made in simple NPZD models, and hence may imply similar limitations. Franks et al. (1986) showed that such simplified ecosystem models nevertheless allow the realistic simulation of the first-order response of primary producers to main environmental conditions. The present ice alga model responds primarily to light availability (driven by incident irradiance and sea-ice and snow thicknesses), as well as to nutrient availability (driven by the ocean hydrodynamics), leading to a seasonal evolution, and ice algal and faunal biomass levels that compare well with previous observations on the HBS, although those observations were limited to nearshore areas (i.e., James Bay, Manitousuk Sound and Chesterfield Inlet). The first important result highlighted by the coupled simulation is the marked west–east gradient in ice algal production in Hudson Bay. Low ice algal production ($<1 \text{ g C m}^{-2} \text{ year}^{-1}$) in the eastern part of the Hudson Bay results from greater ice thickness a result of drifting ice accumulation and low nutrient concentrations in this area, caused by a strong freshwater influence. The low

simulated ice algal biomass ($5\text{--}15\text{ mg Chl}a\text{ m}^{-2}$) in the east agrees with previous observations made in the Manitounuk Sound region near the mouth of the Great Whale River, where the ice algal biomass never exceeded $20\text{--}40\text{ mg Chl}a\text{ m}^{-2}$ (Gosselin et al. 1986; Tremblay et al. 1989; Michel et al. 1993; Legendre et al. 1996; Monti et al. 1996) or in the James Bay (D. Messier, Hydro-Québec, pers. comm.). On a smaller scale than the simulated one, a marked cross-shore gradient of ice algal productivity was previously observed in the region of the Great Whale River (Ingram & Larouche 1987; Larouche & Galbraith 1989; Legendre et al. 1996), which is associated with the salinity gradient of the river plume. On the contrary, western Hudson Bay is subject to wind-driven export of sea ice that causes the formation of a latent heat polynya. In the marginal zone of this nearshore polynya, the thin ice cover and associated high nutrient concentrations (as a result of water mixing by wind action) are ideal conditions for ice algal growth, explaining the high ice algal productions simulated in this area. These high productivity and biomass accumulations agree with previous observations by Welch et al. (1991) of ice algal biomass greater than $100\text{ mg Chl}a\text{ m}^{-2}$ offshore of Chesterfield Inlet in March–May.

The same pattern at a smaller scale is also simulated in Foxe Basin, with a decreasing gradient of ice algal productivity from west to east. Environmental conditions of the more productive western Foxe Basin can be first compared with those encountered in the northern Canadian Archipelago, such as Barrow Strait or Resolute Passage, where high ice algal biomasses ($>100\text{ mg Chl}a\text{ m}^{-2}$) have been observed (Michel et al. 1996). The Foxe Basin area is also subject to some wind-driven transport of sea ice, causing the formation of a latent heat polynya like, although smaller, that of the western Hudson Bay. Eastern Foxe Basin is known as an ice accumulation area, with ice thicknesses frequently greater than 3 m and melting that occurs late in summer. Relatively high nutrient concentrations in this area indicate that ice algal productivity is primarily light-limited in spring. The rapid ice melt in summer limits biomass accumulation by sloughing later in the season, i.e., when light is no longer limiting, leading to a shortened ice algal bloom and, consequently, a moderate mean productivity (Fig. 10). This suggests that, in addition to favourable light (i.e., moderate ice cover) and nutrient conditions, there exists an “optimal window” for ice algal production driven by a sufficient time lag between the period of increasing light and the period of ice-melt. Nutrient limitation affects the photoacclimation capacity of the ice algae, leading to a delayed bloom and, consequently, to a shortened optimal window. This indirect effect of nutrient limitation may also be of importance for the low produc-

tivity of eastern Hudson Bay. Similarly, Jin et al. (2006) describe a three-stage scenario of the ice algal bloom for landfast ice offshore of Barrow (Alaska), and relate inter-annual variations of the ice ecosystem production to match/mismatch the last two stages: the bloom and the ice melt sloughing of ice algae. By shortening this “optimal window”, the earlier ice melt observed in Hudson Bay since the 1980s (Gagnon & Gough 2005a,b; Stirling & Parkinson 2006), and in other Arctic regions, would be more damaging for ice algal production than a later freezing, which would affect the productive season to a lesser extent.

To our knowledge, no observations are available for the winter–spring ice algal production in the Hudson Strait and Ungava Bay region. Hudson Strait is a very dynamic area, with high nutrient concentrations and a moderate and variable ice cover that would favour ice algal production. Ungava Bay represents another favourable location, with moderate ice thickness and a constant replenishment of nutrients in the upper water column to sustain high levels of ice algal primary production. In our simulation, the continuous nutrient input is driven by strong tidal mixing and nutrient-rich water entering Hudson Strait from the Labrador Sea and Frobisher Bay, before transiting through Ungava Bay. The lowest values of ice algal annual primary production, in nearshore and freshwater-influenced areas east of Hudson Bay, are similar to estimates made in the Baltic Sea (Haecky & Andersson 1999), or in northern fjords with long-lasting and thick ice and snow cover (e.g., Mikkelsen et al. 2008). The higher values observed in the nutrient-rich region of the HBS (up to $300\text{ mg C m}^{-2}\text{ day}^{-1}$ or $20\text{--}25\text{ g C m}^{-2}\text{ year}^{-1}$) are in the range of daily estimates (see Mock & Gradinger 1999: table 2) or annual estimates from the Canadian Archipelago (Smith et al. 1988; Michel et al. 2006).

Therefore, the high spatial variability seen in the simulation could be realistic considering the variety of conditions found in the HBS. Indeed, ice algae and associated grazers are known to be highly patchy, with spatial scales of variability ranging from tens of metres, as a result of uneven snow cover or the thermal and optical properties of ice (e.g., Gosselin et al. 1986; Mundy et al. 2005), to a few kilometres or more, depending on the underlying oceanic variability (Gosselin et al. 1986; Granskog et al. 2005). Moreover, the poor response of the ice alga model to snow cover, which does not show marked subregional variability because of a rapid snow/ice compaction in the sea-ice model, suggests that the spatial variability is certainly still under-represented. This variability makes it difficult to reasonably forecast the ice algal production on the regional scale from observations only (e.g., McMinn & Hegseth 2007). This study is the first to give an estimate of the ice algal primary produc-

tion over the whole HBS with respect to the local to mesoscale spatiotemporal variability of environmental conditions encountered in the system. Averaged over the whole HBS, the yearly integrated ice algal primary production is $3.7 \text{ g C m}^{-2} \text{ year}^{-1}$, close to previous estimates for Hudson Bay (Legendre et al. 1992) or other Arctic regions (e.g., Gosselin et al. 1997; Hegseth 1998; Sakshaug 2004; Jin et al. 2006; Lee et al. 2008). This estimate of sea-ice primary production would represent 10–15% of the total primary production of the system that was previously estimated to be between 24 (Roff & Legendre 1986) and $50\text{--}70 \text{ g C m}^{-2} \text{ year}^{-1}$ (Sakshaug 2004). It is also in the range of previous observations in other areas where ice algal production can reach up to 25% of the total primary production (Legendre et al. 1992; Hegseth 1998; Arrigo & Thomas 2004).

The release of POM from the ice ecosystem represents, on average, nearly half of the primary production on an annual basis, as part of the primary production results from regeneration of nutrients in the model through the fraction (70%) of ingested but not assimilated algal biomass by grazers. Assuming that this POM represents new primary production (in the classical sense), this would be a reasonable value considering the non-linearity between primary production and nutrient regeneration in the model. This point was verified with the set-up model by estimating the fraction of the total ice algal production resulting from regenerated production. Our simulation indicates that regenerated production contributes to 40% of the total annual ice algal production. After its release into the water column, the simulation shows a large redistribution of POM (Fig. 12) by the general circulation, whereas < 5%, on average, reaches the seafloor (Fig. 13), where it can be used by benthic organisms or is sequestered into the sediment. Local phenomena such as gyres or the local topography (deeper areas) greatly increase depth-integrated POM concentrations (e.g., in the centre of Hudson Bay in June–July; Fig. 12), and the residence time of POM in the water column before its deposition on the seafloor. This leads to some uncoupling between the spatial distribution of the yearly integrated primary production and sediment accumulation in deeper areas (Fig. 13), i.e., the centre of the bay and Hudson Strait, whereas shallow areas show more coherent patterns (except Ungava Bay, which is subject to strong tidal mixing). This long residence time of the released POM in the water column is caused by the quadratic sinking rates used in the model. The enhancement of the vertical stratification of the water column just after sea-ice melt, through changes in buoyancy (not included in the model) or tidal and vertical mixing (included in the model), can also contribute to change the residence time of POM in the water column.

These results are nevertheless consistent with previous studies in the Canadian Archipelago, where Michel et al. (1996) observed that about 70% of the ice-produced POM was still suspended in the water column 1 month after the bloom, or in the Beaufort Sea, where Carey (1987) observed that less than 10% of the ice algal production reached the benthos during the production period. More direct coupling between ice algal production and the benthos compartment is generally observed in shallower marine systems, such as the Baltic Sea (e.g., Haecky et al. 1998). The fate of this POM ultimately depends on the pelagic ecosystem, and how it would react to this flow of available organic matter or living ice diatoms just prior to the summer plankton bloom. We note that the modelled ice algal production and biomass in our study agreed for the most part with observations in the HBS and the nearby Arctic region. The present model will be coupled in the near future to a planktonic model in order to obtain a more complete view of the HBS ecosystem functioning, and to predict its response to climate warming.

Acknowledgements

This work was supported by an Academic Grant to BZ from Fisheries and Oceans Canada, a Discovery Grant to FJS from the Natural Sciences and Engineering Research Council, and a travel award and scholarship to VS from the ISMER Scholarship Program, ArcticNet and Québec Ocean. The authors gratefully acknowledge the technical contribution of J. Caveen, who helped with model development and associated numerical and graphical tools. We thank the “MERICA” research team from Fisheries and Oceans Canada and D. Messier from Hydro-Québec for providing data and for fruitful discussions on the results. We also thank Laure Devine for linguistic revision of the manuscript, and A. McMinn and K. Denman for their constructive comments and suggestions that improved the manuscript. Finally, we hope this paper will honour the memory of our colleague and friend François J. Saucier, who died in 2008, and who always loved so to see a little life colonizing his ice–ocean model.

References

- Anderson G.C., Parsons T.R. & Stephens K. 1969. Nitrate distribution in the subarctic Northeast Pacific Ocean. *Deep-Sea Research* 16, 329–334.
- Arrigo K.R. 2003. Primary production in sea ice. In D.N. Thomas & G.S. Dieckmann (eds.): *Sea ice: an introduction to its physics, chemistry, biology and geology*. Pp. 143–183. Oxford: Blackwell Science.

- Arrigo K.R., Kremer J.N. & Sullivan C.W. 1993. A simulated fast ice ecosystem. *Journal of Geophysical Research—Oceans* 98, 6929–6946.
- Arrigo K.R. & Sullivan C.W. 1994. A high resolution bio-optical model of microalgal growth: tests using sea ice algal community time-series data. *Limnology and Oceanography* 39, 609–631.
- Arrigo K.R. & Thomas D.N. 2004. Large scale importance of sea ice biology in the Southern Ocean. *Antarctic Science* 16, 471–486.
- Booth J.A. 1984. The epontic algal community of the ice edge zone and its significance to the Davis Strait ecosystem. *Arctic* 37, 234–243.
- Carey A.G. Jr. 1987. Particle flux beneath fast ice in the shallow southwestern Beaufort Sea, Arctic Ocean. *Marine Ecology Progress Series* 40, 247–257.
- Carmack E., Barber D., Christensen J., Macdonald R., Rudels B. & Sakshaug E. 2006. Climate variability and physical forcing of the food webs and the carbon budget on antarctic shelves. *Progress in Oceanography* 71, 145–181.
- Cloern J.E. 1995. An empirical model of the phytoplankton chlorophyll : carbon ratio—the conversion factor between productivity and growth rate. *Limnology and Oceanography* 40, 1313–1321.
- Comiso J.C., Parkinson C.L., Gersten R. & Stock L. 2008. Accelerated decline in the Arctic sea ice cover. *Geophysical Research Letters* 35, L01603, doi: 10.1029/2007GL031972.
- Conover R.J., Herman A.W., Prinsenberg S.J. & Harris L.R. 1986. Distribution of and feeding by the copepod *Pseudocalanus* under fast ice during the Arctic spring. *Science* 232, 1245–1247.
- Conover R.J. & Huntley M. 1991. Copepods in ice-covered seas—distribution, adaptations to seasonally limited food, metabolism, growth patterns and life cycle strategies in polar seas. *Journal of Marine Systems* 2, 1–41.
- Cota G.F. 1985. Photoadaptation of High Arctic ice algae. *Nature* 315, 219–222.
- Cota G.F., Legendre L., Gosselin M. & Ingram R.G. 1991. Ecology of bottom ice algae: I. Environmental controls and variability. *Journal of Marine Systems* 2, 257–277.
- Cota G.F., Prinsenberg S.J., Bennett E.B., Loder J.W., Lewis M.R., Anning J.L., Watson N.H.F. & Harris L.R. 1987. Nutrient fluxes during extended blooms of Arctic ice algae. *Journal of Geophysical Research—Oceans* 92, 1951–1962.
- Cota G.F. & Smith R.E.H. 1991a. Ecology of bottom ice algae: 2. Dynamics, distributions and productivity. *Journal of Marine Systems* 2, 279–295.
- Cota G.F. & Smith R.E.H. 1991b. Ecology of bottom ice algae: 3. Comparative physiology. *Journal of Marine Systems* 2, 297–315.
- Cota G.F. & Sullivan C.W. 1990. Photoadaptation, growth and production of bottom ice algae in the Antarctic. *Journal of Phycology* 26, 399–411.
- Demers S., Legendre L., Maestrini S.Y., Rochet M. & Ingram R.G. 1989. Nitrogenous nutrition of sea ice microalgae. *Polar Biology* 9, 377–383.
- Droop M.R. 1983. 25 years of algal growth kinetics. *Botanica Marina* 26, 99–112.
- Edwards A.M. & Bees M.A. 2001. Generic dynamics of a simple plankton population model with a non-integer exponent of closure. *Chaos, Solitons and Fractals* 12, 289–300.
- Eicken H. 2003. Chapter 2. From the microscopic, to the macroscopic, to the regional scale: growth, microstructure and properties of sea ice. In D.N. Thomas & G.S. Dieckmann (eds.): *Sea ice: an introduction to its physics, chemistry, biology and geology*. Pp. 22–81. Oxford: Blackwell Science.
- Fortier M., Fortier L., Michel C. & Legendre L. 2002. Climatic and biological forcing of the vertical flux of biogenic particles under seasonal Arctic sea ice. *Marine Ecology Progress Series* 225, 1–16.
- Franks P.J.S., Wroblewski J.S. & Flierl G.R. 1986. Behavior of a simple plankton model with food-level acclimation by herbivores. *Marine Biology* 91, 121–129.
- Gagnon A.S. & Gough W.A. 2005a. Climate change scenarios for the Hudson Bay region: an intermodel comparison. *Climatic Change* 69, 269–297.
- Gagnon A.S. & Gough W.A. 2005b. Trends in the dates of ice freeze-up and breakup over Hudson Bay, Canada. *Arctic* 58, 370–382.
- Geider R.J., MacIntyre H.L. & Kana T.M. 1997. Dynamic model of phytoplankton growth and acclimation: responses of the balanced growth rate and the chlorophyll *a* : carbon ratio to light, nutrient-limitation and temperature. *Marine Ecology Progress Series* 148, 187–200.
- Gosselin M., Legendre L., Demers S. & Ingram R.G. 1985. Responses of sea ice microalgae to climatic and fortnightly tidal energy inputs (Manitounuk Sound, Hudson Bay). *Canadian Journal of Fisheries and Aquatic Sciences* 42, 999–1006.
- Gosselin M., Legendre L., Therriault J.C. & Demers S. 1990. Light and nutrient limitation of sea ice microalgae (Hudson Bay, Canadian Arctic). *Journal of Phycology* 26, 220–232.
- Gosselin M., Legendre L., Therriault J.C., Demers S. & Rochet M. 1986. Physical control of the horizontal patchiness of sea ice microalgae. *Marine Ecology Progress Series* 29, 289–298.
- Gosselin M., Levasseur M., Wheeler P.A., Horner R.A. & Booth B.C. 1997. New measurements of phytoplankton and ice algal production in the Arctic Ocean. *Deep-Sea Research Part II* 44, 1623–1644.
- Gradinger R. 1996. Occurrence of an algal bloom under Arctic pack ice. *Marine Ecology Progress Series* 131, 301–305.
- Gradinger R. 2009. Sea-ice algae: major contributors to primary production and algal biomass in the Chukchi and Beaufort seas during May/June 2002. *Deep Sea Research Part II* 56, 1201–1212.
- Gradinger R. & Ikävalko J. 1998. Organism incorporation into newly forming Arctic sea ice in the Greenland Sea. *Journal of Plankton Research* 20, 871–886.

- Gradinger R., Spindler M. & Henschel D. 1991. Development of Arctic sea ice organisms under graded snow cover. *Polar Research* 10, 295–307.
- Grainger E.H., Lovrity J.E. & Evans M.S. 1977. *Biological oceanographic observations in the Eskimo Lakes, Arctic Canada. Physical, nutrient and primary production data, 1961–1975. Fisheries and Marine Service Technical Report 685.* Sainte-Anne-de-Bellevue: Environment Canada.
- Granskog M.A. 1999. Baltic sea ice as a medium for storage of particulate matter and elements. *ICES Journal of Marine Science* 56, 172–175.
- Granskog M.A., Kaartokallio H., Kuosa H., Thomas D.N., Ehn J. & Sonninen E. 2005. Scales of horizontal patchiness in chlorophyll *a*, chemical and physical properties of landfast sea ice in the Gulf of Finland (Baltic Sea). *Polar Biology* 28, 276–283.
- Grebmeier J.M., Overland J.E., Moore S.E., Farley E.V., Carmack E.C., Cooper L.W., Frey K.E., Helle J.H., McLaughlin F.A. & McNutt S. 2006. A major ecosystem shift in the northern Bering Sea. *Science* 311, 1461–1464.
- Haecy P. & Andersson A. 1999. Primary and bacterial production in sea ice in the northern Baltic Sea. *Aquatic Microbial Ecology* 20, 107–118.
- Haecy P., Jonsson S. & Andersson A. 1998. Influence of sea ice on the composition of the spring phytoplankton bloom in the northern Baltic Sea. *Polar Biology* 20, 1–8.
- Hall R.T. & Rothrock D.A. 1987. Photogrammetric observations of the lateral melt of sea ice floes. *Journal of Geophysical Research—Oceans* 92, 7045–7048.
- Hansen P.J., Bjornsen P.K., Hansen B.W. 1997. Zooplankton grazing and growth: scaling within the 2–2000- μm body size range. *Limnology and Oceanography* 42, 687–704.
- Hegseth E.N. 1992. Sub-ice algal assemblages of the Barents Sea: species composition, chemical composition, and growth rates. *Polar Biology* 12, 485–496.
- Hegseth E.N. 1998. Primary production of the northern Barents Sea. *Polar Research* 17, 113–123.
- Hegseth E.N. & von Quillfeldt C.H. 2002. Low phytoplankton biomass and ice algal blooms in the Weddell Sea during the ice-filled summer of 1997. *Antarctic Science* 14, 231–243.
- Holland M.M. & Bitz C.M. 2003. Polar amplification of climate change in coupled models. *Climate Dynamics* 21, 221–232.
- Horner R.A. & Schrader G.C. 1982. Relative contributions of ice algae, phytoplankton, and benthic microalgae to primary production in nearshore regions of the Beaufort Sea. *Arctic* 35, 484–503.
- Hudon C., Morin R., Bunch J. & Harland R. 1996. Carbon and nutrient output from the Great Whale River (Hudson Bay) and a comparison with other rivers around Quebec. *Canadian Journal of Fisheries and Aquatic Sciences* 53, 1513–1525.
- Hunke E.C. & Dukowicz J.K. 1997. An elastic–viscous–plastic model for sea ice dynamics. *American Meteorological Society* 77, 1849–1867.
- Ikävalko J. & Thomsen H.A. 1997. The Baltic Sea ice biota (March 1994): a study of the protistan community. *European Journal of Protistology* 33, 229–243.
- IMBER (Integrated Marine Biogeochemistry and Ecosystem Research) 2005. *Science plan and implementation strategy. IGBP Report 52.* Stockholm: International Geosphere–Biosphere Programme Secretariat.
- Ingram R.G. & Larouche P. 1987. Under-ice characteristics of the La Grande River plume due to discharge variations. *Atmosphere–Ocean* 25, 242–250.
- Ingram R.G., Osler J.C. & Legendre L. 1989. Influence of internal wave induced vertical mixing on ice algal production in a highly stratified sound. *Estuarine, Coastal and Shelf Science* 29, 435–446.
- Ingram R.G. & Prinsenberg S. 1998. Coastal oceanography of Hudson Bay and surrounding eastern Canadian Arctic waters coastal segment (26,P). In A.R. Robinson & K.H. Brink (eds.): *The sea: ideas and observation on progress in the study of the seas*. Pp. 835–859. New York: John Wiley and Sons.
- Ingram R.G., Wang J., Lin C., Legendre L. & Fortier L. 1996. Impact of freshwater on a subarctic coastal ecosystem under seasonal sea ice (southeastern Hudson Bay, Canada). I. Interannual variability and predicted global warming influence on river plume dynamics and sea ice. *Journal of Marine Systems* 7, 221–231.
- Jin M., Deal C.J., Wang J., Alexander V., Gradinger R.R., Saitoh S., Iida T., Wan Z. & Stabenro P. 2007. Ice-associated phytoplankton blooms in the southeastern Bering Sea. *Geophysical Research Letters* 34, L06612, doi: 10.1029/2006GL028849.
- Jin M., Deal C.J., Wang J., Shin K.H., Tanaka N., Whitlege T.E., Lee S.H. & Gradinger R.R. 2006. Controls of the landfast ice–ocean ecosystem offshore Barrow, Alaska. *Annals of Glaciology* 44, 63–72.
- Kaartokallio H. 2001. Evidence for active microbial nitrogen transformations in sea ice (Gulf of Bothnia, Baltic Sea) in midwinter. *Polar Biology* 24, 21–28.
- Kaartokallio H. 2004. Food web components, and physical and chemical properties of Baltic Sea ice. *Marine Ecology Progress Series* 273, 49–63.
- Kirst G.O. & Wiencke C. 1995. Ecophysiology of polar algae. *Journal of Phycology* 31, 181–199.
- Krembs C., Gradinger R. & Spindler M. 2000. Implications of brine channel geometry and surface area for the interaction of sympagic organisms in Arctic sea ice. *Journal of Experimental Marine Biology and Ecology* 243, 55–80.
- Krembs C., Tuschling K. & Juterzenka K.V. 2002. The topography of the ice–water interface—its influence on the colonization of sea ice by algae. *Polar Biology* 25, 106–117.
- Kudoh S. 1995. Characteristics of sea ice algal community and the primary production in Saroma Ko Lagoon and Resolute Passage, 1992 (extended abstract). *Proceedings of the NIPR Symposium on Polar Biology* 8, 54–56.
- Larouche P. & Galbraith P.S. 1989. Factors affecting fast ice consolidation in southeastern Hudson Bay, Canada. *Atmosphere–Ocean* 27, 367–375.

- Laurion I., Demers S. & Vezina A.F. 1995. The microbial food web associated with the ice algal assemblage: biomass and bacterivory of nanoflagellate protozoans in Resolute Passage (High Canadian Arctic). *Marine Ecology Progress Series* 120, 77–87.
- Lavoie D., Denman K. & Michel C. 2005. Modeling ice algal growth and decline in a seasonally ice-covered region of the Arctic (Resolute Passage, Canadian Archipelago). *Journal of Geophysical Research—Oceans* 110, C11009, doi: 10.1029/2005JC002922.
- Lavoie D., Macdonald R.W. & Denman K.L. 2008. Primary productivity and export fluxes on the Canadian shelf of the Beaufort Sea: a modelling study. *Journal of Marine Systems* 75, 17–32.
- LeBlond P.H., Osborne T.M., Hodgins D.O., Goodman R. & Metge M. 1981. Surface circulation in the western Labrador Sea. *Deep-Sea Research Part I* 28, 683–693.
- Lee S.H., Whitledge T.E. & Kang S.-H. 2008. Spring time production of bottom ice algae in the landfast sea ice zone at Barrow, Alaska. *Journal of Experimental Marine Biology and Ecology* 367, 204–212.
- Le Fèvre J., Legendre L. & Rivkin R.B. 1998. Fluxes of biogenic carbon in the Southern Ocean: roles of large microphagous zooplankton. *Journal of Marine Systems* 17, 325–345.
- Legendre L., Martineau M.J., Therriault J.C. & Demers S. 1992. Chlorophyll *a* biomass and growth of sea ice microalgae along a salinity gradient (southeastern Hudson Bay, Canadian Arctic). *Polar Biology* 12, 445–453.
- Legendre L., Robineau B., Gosselin M., Michel C., Ingram R.G., Fortier L., Therriault J.C., Demers S. & Monti D. 1996. Impact of freshwater on a subarctic coastal ecosystem under seasonal sea ice (southeastern Hudson Bay) 2. Production and export of microalgae. *Journal of Marine Systems* 7, 223–250.
- Lindsay R.W. & Zhang J. 2005. The thinning of Arctic sea ice, 1988–2003: have we passed a tipping point? *Journal of Climate* 18, 4879–4894.
- Lizotte M.P. 2001. The contributions of sea ice algae to Antarctic marine primary production. *American Zoologist* 41, 57–73.
- Lizotte M.P. 2003. The microbiology of sea ice. In D.N. Thomas & G.S. Dieckmann (eds.): *Sea ice: an introduction to its physics, chemistry, biology and geology*. Pp. 184–210. Oxford: Blackwell Science.
- Lytle V.I. & Ackley S.F. 1996. Heat flux through sea ice in the western Weddell Sea: convective and conductive transfer processes. *Journal of Geophysical Research—Oceans* 101, 8853–8868.
- MacIntyre H.L., Kana T.M., Anning T. & Geider R.J. 2002. Photoacclimation of photosynthesis irradiance response curves and photosynthetic pigments in microalgae and cyanobacteria. *Journal of Phycology* 38, 17–38.
- Maestrini S.Y., Rochet M., Legendre L. & Demers S. 1986. Nutrient limitation of the bottom-ice microalgal biomass (southeastern Hudson Bay, Canadian Arctic). *Limnology and Oceanography* 31, 969–982.
- Manabe S., Milly P.C.D. & Wetherald R. 2004. Simulated long-term changes in river discharge and soil moisture due to global warming. *Hydrological Sciences Journal* 49, 625–642.
- Martini I.P. 1986. *Canadian inland seas*. Amsterdam: Elsevier.
- Matsumoto K., Takanezawa T. & Ooe M. 2000. Ocean tide models developed by assimilating TOPEX/POSEIDON altimeter data into hydrodynamical model: a global model and a regional model around Japan. *Journal of Oceanography* 56, 567–581.
- McMinn A. & Hegseth E.N. 2007. Sea ice primary productivity in the northern Barents Sea, spring 2004. *Polar Biology* 30, 289–294.
- McMinn A., Ryan K.G., Ralph P.J. & Pankowski A. 2007. Spring sea ice photosynthesis, primary productivity and biomass distribution in eastern Antarctica, 2002–2004. *Marine Biology* 151, 985–995.
- Michel C., Ingram R.G. & Harris L.R. 2006. Variability in oceanographic and ecological processes in the Canadian Arctic Archipelago. *Progress in Oceanography* 71, 379–401.
- Michel C., Legendre L., Demers S. & Therriault J.C. 1988. Photoadaptation of sea ice microalgae in springtime: photosynthesis and carboxylating enzymes. *Marine Ecology Progress Series* 50, 177–185.
- Michel C., Legendre L., Ingram R.G., Gosselin M. & Levasseur M. 1996. Carbon budget of sea ice algae in spring: evidence of a significant transfer to zooplankton grazers. *Journal of Geophysical Research—Oceans* 101, 18 345–18 360.
- Michel C., Legendre L., Therriault J.C., Demers S. & Vandavelde T. 1993. Springtime coupling between ice algal and phytoplankton assemblages in southeastern Hudson Bay, Canadian Arctic. *Polar Biology* 13, 441–449.
- Michel C., Nielsen T.G., Nozais C. & Gosselin M. 2002. Significance of sedimentation and grazing by ice micro- and meiofauna for carbon cycling in annual sea ice (northern Baffin Bay). *Aquatic Microbial Ecology* 30, 57–68.
- Mikkelsen D.M., Rysgaard S. & Glud R.N. 2008. Microalgal composition and primary production in Arctic sea ice: a seasonal study from Kobbefjord (Kangerluarsunnguaq), West Greenland. *Marine Ecology Progress Series* 368, 65–74.
- Mock T. & Gradinger R. 1999. Determination of Arctic ice algal production with a new in situ incubation technique. *Marine Ecology Progress Series* 177, 15–26.
- Mock T. & Gradinger R. 2000. Changes in photosynthetic carbon allocation in algal assemblages of Arctic sea ice with decreasing nutrient concentrations and irradiance. *Marine Ecology Progress Series* 202, 1–11.
- Moline M.A., Karnovsky N.J., Brown Z., Divoky G.J., Frazer T.K., Jacoby C.A., Torres J.J. & Fraser W.R. 2008. High latitude changes in ice dynamics and their impact on polar marine ecosystems. *Annals of the New York Academy of Sciences* 1134, 267–319.
- Monti D., Legendre L., Therriault J.-C. & Demers S. 1996. Horizontal distribution of sea ice microalgae: environmental control and spatial processes (southeastern

- Hudson Bay, Canada). *Marine Ecology Progress Series* 133, 229–240.
- Morison J., Aagaard K. & Steele M. 2000. Recent environmental changes in the Arctic: a review. *Arctic* 54, 359–371.
- Mundy C.J., Barber D.G. & Michel C. 2005. Variability of snow and ice thermal, physical and optical properties pertinent to sea ice algae biomass during spring. *Journal of Marine Systems* 58, 107–120.
- Mundy C.J., Barber D.G., Michel C. & Marsden R.F. 2007. Linking ice structure and microscale variability of algal biomass in Arctic first-year sea ice using an in situ photographic technique. *Polar Biology* 30, 1099–1114.
- Nechaev D., Yaremchuk M. & Ikeda M. 2004. Decadal variability of circulation in the Arctic Ocean retrieved from climatological data by a variational method. *Journal of Geophysical Research—Oceans* 109, C04006, doi: 10.1029/2002JC001740.
- Nishi Y. & Tabeta S. 2005. Analysis of the contribution of ice algae to the ice-covered ecosystem in Lake Saroma by means of a coupled ice–ocean ecosystem model. *Journal of Marine Systems* 55, 249–279.
- Nishi Y. & Tabeta S. 2007. Sunlight and tidal interaction as a mechanism of carbon transport in an ice-covered region: Results of a coupled ice–ocean ecosystem model. *Continental Shelf Research* 27, 1–19.
- Nishi Y. & Tabeta S. 2008. Relation of material exchange between sea ice and water to a coupled ice–ocean ecosystem at the Hokkaido coastal region of the Okhotsk Sea. *Journal of Geophysical Research—Oceans* 113, C01003, doi: 10.1029/2006JC004077.
- Nozais C., Gosselin M., Michel C. & Tita G. 2001. Abundance, biomass, composition and grazing impact of the sea ice meiofauna in the North Water, northern Baffin Bay. *Marine Ecology Progress Series* 217, 235–250.
- Perovich D.K. 1996. *The optical properties of sea ice. CRREL Monograph 96-1*. Springfield, VA: US Army Corps of Engineers, Cold Regions Research and Engineering Laboratory.
- Platt T., Gallegos C.L. & Harrison W.G. 1980. Photoinhibition of photo-synthesis in natural assemblages of marine phytoplankton. *Journal of Marine Research* 38, 687–701.
- Poulin M. & Cardinal A. 1982. Sea ice diatoms from Manitounuk Sound, southeastern Hudson Bay (Quebec, Canada). II. Naviculaceae, genus *Navicula*. *Canadian Journal of Botany* 60, 2825–2845.
- Poulin M. & Cardinal A. 1983. Sea ice diatoms from Manitounuk Sound, southeastern Hudson Bay (Quebec, Canada). III. Cymbellaceae, Entomoneidaceae, Gomphonemataceae, and Nitzschiaceae. *Canadian Journal of Botany* 61, 107–111.
- Prinsenberg S.J. 1986. The circulation pattern and current structure of Hudson Bay. In I.P. Martini (ed.): *Canadian inland seas*. Pp. 187–204. Amsterdam: Elsevier.
- Prinsenberg S.J. 1988. Ice-cover and ice-ridge contributions to the freshwater contents of Hudson Bay and Foxe Basin. *Arctic* 41, 6–11.
- Riedel A., Michel C., Gosselin M. & LeBlanc B. 2007. Enrichment of nutrients, exopolymeric substances and microorganisms in newly formed sea ice on the Mackenzie shelf. *Marine Ecology Progress Series* 342, 55–67.
- Robinson D.H., Arrigo K.R., Kolber Z., Gosselin M. & Sullivan C.W. 1998. Photophysiological evidence of nutrient limitation of platelet ice algae in McMurdo Sound, Antarctica. *Journal of Phycology* 34, 788–797.
- Roff J. & Legendre L. 1986: Physico-chemical and biological oceanography of Hudson Bay. In I.P. Martini (ed.): *Canadian inland seas*. Pp. 265–292. Amsterdam: Elsevier.
- Rozanska M., Poulin M. & Gosselin M. 2008. Protist entrapment in newly formed sea ice in the Coastal Arctic Ocean. *Journal of Marine Systems* 74, 887–901.
- Rozanska M., Gosselin M., Poulin M., Wiktor J.F. & Michel C. 2009. Influence of environmental factors on the development of bottom ice protist communities during the winter–spring transition. *Marine Ecology Progress Series* 386, 43–59.
- Runge J.A. & Ingram R.G. 1988. Underice grazing by planktonic, calanoid copepods in relation to a bloom of ice microalgae in southeastern Hudson Bay. *Limnology and Oceanography* 33, 280–286.
- Runge J.A., Therriault J.-C., Legendre L., Ingram R.G. & Demers S. 1991. Coupling between ice microalgal productivity and the pelagic, metazoan food web in southeastern Hudson Bay: a synthesis of results. *Polar Research* 10, 325–338.
- Sakshaug E. 2004. Primary and secondary production in the Arctic seas. In R. Stein & R.W. Macdonald (eds.): *The organic carbon cycle in the Arctic Ocean*. Pp. 366. Berlin: Springer.
- Saucier F.J., Senneville S., Prinsenberg S., Roy F., Smith G., Gachon P., Caya D. & Laprise R. 2004. Modelling the sea ice–ocean seasonal cycle in Hudson Bay, Foxe Basin and Hudson Strait, Canada. *Climate Dynamics* 23, 303–326.
- Schnack-Schiel S.B. 2003. The macrobiology of sea ice. In D.N. Thomas & G.S. Dieckmann (eds.): *Sea ice: an introduction to its physics, chemistry, biology and geology*. Pp. 211–239. Oxford: Blackwell Science.
- Semtner A.J. Jr. 1976. A model for the thermodynamic growth of sea ice in numerical investigations of climate. *Journal of Physical Oceanography* 6, 379–389.
- Sirevaag A. 2009. Turbulent exchange coefficients for the ice/ocean interface in case of rapid melting. *Geophysical Research Letters* 36, L04606, doi: 10.1029/2008GL036587.
- Smetacek V. & Nicol S. 2005. Polar ocean ecosystems in a changing world. *Nature* 437, 362–368.
- Smith R.C., Anning J., Clement P. & Cota G. 1988. Abundance and production of ice algae in Resolute Passage, Canadian Arctic. *Marine Ecology Progress Series* 48, 251–263.
- Smith R.E.H., Harrison W.G., Harris L.R. & Herman A.W. 1990. Vertical fine structure of particulate matter and nutrients in sea ice of the High Arctic. *Canadian Journal of Fisheries and Aquatic Sciences* 47, 1348–1355.

- Smith R.E.H., Gosselin M. & Taguchi S. 1997. The influence of major inorganic nutrients on the growth and physiology of High Arctic ice algae. *Journal of Marine Systems* 11, 63–70.
- Stirling I. & Parkinson C.L. 2006. Possible effects of climate warming on selected populations of polar bears (*Ursus maritimus*) in the Canadian Arctic. *Arctic* 59, 261–275.
- Straneo F. & Saucier F.J. 2008. The outflow from Hudson Strait and its contribution to the Labrador Current. *Deep-Sea Research Part I* 55, 926–946.
- Suzuki Y., Kudoh S. & Takahashi M. 1997. Photosynthetic and respiratory characteristics of an Arctic ice algal community living in low light and low temperature conditions. *Journal of Marine Systems* 11, 111–121.
- Tremblay C., Runge J.A. & Legendre L. 1989. Grazing and sedimentation of ice algae during and immediately after a bloom at the ice–water interface. *Marine Ecology Progress Series* 56, 291–300.
- von Quillfeldt C.H., Ambrose W.G. Jr. & Clough L.M. 2003. High number of diatom species in first-year ice from the Chukchi Sea. *Polar Biology* 26, 806–818.
- Wassmann P., Carroll J. & Bellerby R.G.J. 2008. Carbon flux and ecosystem feedback in the northern Barents Sea in an era of climate change: an introduction. *Deep-Sea Research Part II* 55, 2143–2153.
- Welch H.E., Bergmann M.A., Siferd T.D. & Amarualik P.S. 1991. Seasonal development of ice algae near Chesterfield Inlet, N.W.T., Canada. *Canadian Journal of Fisheries and Aquatic Sciences* 48, 2395–2402.
- Werner I. 1997. Grazing of Arctic under-ice amphipods on sea ice algae. *Marine Ecology Progress Series* 160, 93–99.
- Werner I., Ikävalko J. & Schünemann H. 2007. Sea-ice algae in Arctic pack ice during late winter. *Polar Biology* 30, 1493–1504.
- Wheeler P.A., Gosselin M., Sherr E., Thibault D., Kirchmans D.L., Benner R. & Whitley T.E. 1996. Active cycling of organic carbon in the Central Arctic Ocean. *Nature* 380, 697–699.
- Wiktor J. & Szymelfenig M. 2002. Patchiness of sympagic algae and meiofauna from the fast ice of North Open Water (NOW) Polynya. *Polish Polar Research* 23, 175–184.
- Zeebe R.E., Eicken H., Robinson D.H., Wolf-Gladrow D. & Dieckmann G.S. 1996. Modeling the heating and melting of sea ice through light absorption by microalgae. *Journal of Geophysical Research—Oceans* 101, 1163–1181.